

10-12-2018

## A Neuroimaging Web Interface for Data Acquisition, Processing and Visualization of Multimodal Brain Images

Gabriel M. Lizarraga  
*Florida International University, gliza002@fiu.edu*

Follow this and additional works at: <https://digitalcommons.fiu.edu/etd>



Part of the [Biomedical Commons](#), [Computer and Systems Architecture Commons](#), [Data Storage Systems Commons](#), and the [Neurosciences Commons](#)

---

### Recommended Citation

Lizarraga, Gabriel M., "A Neuroimaging Web Interface for Data Acquisition, Processing and Visualization of Multimodal Brain Images" (2018). *FIU Electronic Theses and Dissertations*. 3855.  
<https://digitalcommons.fiu.edu/etd/3855>

This work is brought to you for free and open access by the University Graduate School at FIU Digital Commons. It has been accepted for inclusion in FIU Electronic Theses and Dissertations by an authorized administrator of FIU Digital Commons. For more information, please contact [dcc@fiu.edu](mailto:dcc@fiu.edu).

FLORIDA INTERNATIONAL UNIVERSITY

Miami, Florida

A NEUROIMAGING WEB INTERFACE FOR DATA ACQUISITION,  
PROCESSING AND VISUALIZATION OF MULTIMODAL BRAIN IMAGES

A dissertation submitted in partial fulfillment of the

requirements for the degree of

DOCTOR OF PHILOSOPHY

in

COMPUTER SCIENCE

by

Gabriel Lizarraga

2018

To: Dean John Volakis  
College of Engineering and Computing

This dissertation, written by Gabriel Lizarraga, and entitled A Neuroimaging Web Interface for Data Acquisition, Processing and Visualization of Multimodal Brain Images, having been approved in respect to style and intellectual content is referred to you for judgment.

We have read this dissertation and recommend that it be approved.

---

Naphtali Rishe

---

Giri Narasimhan

---

Mercedes Cabrerizo

---

David A Loewenstein

---

Malek Adjouadi, Major Professor

Date of Defense: October 12, 2018.

The dissertation of Gabriel Lizarraga is approved.

---

Dean John L. Volakis  
College of Engineering and Computing

---

Andrés G. Gil  
Vice President for Research and Economic Development  
and Dean of the University Graduate School

Florida International University, 2018

© Copyright 2018 by Gabriel Lizarraga

All rights reserved.

## DEDICATION

I dedicate this work to my parents: Gabriel and Celia.

## ACKNOWLEDGMENTS

First, I want to express my gratitude to my mentor, Dr. Malek Adjouadi, director of the CATE lab in Florida international University. He has guided me every step of the way: from my work as an undergraduate student to my Ph.D. endeavors. I became a member of the Center for Advanced Technology and Education (CATE lab) ten years ago and have worked in many projects with other members of the lab. His constant guidance and support have allowed me to develop my potential as a researcher. It is thanks to him that I was able to find a topic of study, and meet other researchers who have provided me with support in my career endeavors.

I also want to thank the other members of my committee, Dr. Naphtali Rishe, Dr. Giri Narasimhan, Dr. Mercedes Cabrerizo, and Dr. David A Loewenstein for the counseling and support they have provided to me during my Ph.D. studies. Dr. Cabrerizo provided me with insights into epilepsy research and Dr. Loewenstein provided me with great help in assessing neuroimaging data in Alzheimer's disease. Furthermore, I would like to thank Dr. Ranjan Duara and Mr. Warren Barker, with the Mount Sinai Medical Center (MSMC) in Miami Beach. They have provided me with invaluable guidance through their feedback and suggestions regarding medical data and all clinical aspects involving Alzheimer's disease.

I am grateful for the continued support from the National Science Foundation (NSF) under NSF grants CNS-1532061, CNS-1551221, HRD- 0833093, CNS-1429345 and CNS-1338922. We greatly appreciate also the support of the Ware Foundation. This research is also supported through the Florida Department of Health, Ed and Ethel

Moore Alzheimer's Disease Research Program, and the 1Florida ADRC (Alzheimer's Disease Research Center) (1P50AG047266-01A1) and R01 AG047649-01A1 (David Loewenstein, PI).

Data collection and sharing for this project was funded by the Alzheimer's Disease Neuroimaging Initiative (ADNI) (National Institutes of Health Grant U01 AG024904) and DOD ADNI (Department of Defense award number W81XWH-12-2-0012). ADNI is funded by the National Institute on Aging, the National Institute of Biomedical Imaging and Bioengineering, and through generous contributions from the following: AbbVie, Alzheimer's Association; Alzheimer's Drug Discovery Foundation; Araclon Biotech; BioClinica, Inc.; Biogen; Bristol-Myers Squibb Company; CereSpir, Inc.; Cogstate; Eisai Inc.; Elan Pharmaceuticals, Inc.; Eli Lilly and Company; EuroImmun; F. Hoffmann-La Roche Ltd and its affiliated company Genentech, Inc.; Fujirebio; GE Healthcare; IXICO Ltd.; Janssen Alzheimer Immunotherapy Research & Development, LLC.; Johnson & Johnson Pharmaceutical Research & Development LLC.; Lumosity; Lundbeck; Merck & Co., Inc.; Meso Scale Diagnostics, LLC.; NeuroRx Research; Neurotrack Technologies; Novartis Pharmaceuticals Corporation; Pfizer Inc.; Piramal Imaging; Servier; Takeda Pharmaceutical Company; and Transition Therapeutics. The Canadian Institutes of Health Research is providing funds to support ADNI clinical sites in Canada. Private sector contributions are facilitated by the Foundation for the National Institutes of Health ([www.fnih.org](http://www.fnih.org)). The grantee organization is the Northern California Institute for Research and Education, and the study is

coordinated by the Alzheimer's Therapeutic Research Institute at the University of Southern California. ADNI data are disseminated by the Laboratory for Neuro Imaging at the University of Southern California.

## ABSTRACT OF THE DISSERTATION

### A NEUROIMAGING WEB INTERFACE FOR DATA ACQUISITION, PROCESSING AND VISUALIZATION OF MULTIMODAL BRAIN IMAGES

by

Gabriel Lizarraga

Florida International University, 2018

Miami, Florida

Professor Malek Adjouadi, Major Professor

Structural and functional brain images are generated as essential modalities for medical experts to learn about the different functions of the brain. These images are typically visually inspected by experts. Many software packages are available to process medical images, but they are complex and difficult to use. The software packages are also hardware intensive. As a consequence, this dissertation proposes a novel Neuroimaging Web Services Interface (NWSI) as a series of processing pipelines for a common platform to store, process, visualize and share data.

The NWSI system is made up of password-protected interconnected servers accessible through a web interface. The web-interface driving the NWSI is based on Drupal, a popular open source content management system. Drupal provides a user-based platform, in which the core code for the security and design tools are updated and patched frequently. New features can be added via modules, while maintaining the core software secure and intact. The webserver architecture allows for the visualization of results and the downloading of tabulated data. Several forms are

available to capture clinical data. The processing pipeline starts with a FreeSurfer (FS) reconstruction of T1-weighted MRI images. Subsequently, PET, DTI, and fMRI images can be uploaded.

The Webserver captures uploaded images and performs essential functionalities, while processing occurs in supporting servers. The computational platform is responsive and scalable. The current pipeline for PET processing calculates all regional Standardized Uptake Value ratios (SUVRs). The FS and SUVR calculations have been validated using Alzheimer's Disease Neuroimaging Initiative (ADNI) results posted at Laboratory of Neuro Imaging (LONI). The NWSI system provides access to a calibration process through the centiloid scale, consolidating Florbetapir and Florbetaben tracers in amyloid PET images. The interface also offers onsite access to machine learning algorithms, and introduces new heat maps that augment expert visual rating of PET images. NWSI has been piloted using data and expertise from Mount Sinai Medical Center, the 1Florida Alzheimer's Disease Research Center (ADRC), Baptist Health South Florida, Nicklaus Children's Hospital, and the University of Miami. All results were obtained using our processing servers in order to maintain data validity, consistency, and minimal processing bias.

## CONTENTS

| CHAPTER  | PAGE |
|--|------|
| 1. Introduction .....  | 1    |
| 1.1 Neuroimaging Web Services Interface and Research Significance.....   | 1    |
| 1.2 General Statement of the Research Area .....   | 5    |
| 1.3 Research Purpose .....   | 5    |
| 1.4 Significance of the Research.....  | 6    |
| 1.5 Structure of the Research .....  | 6    |
| 2. Related Work and Retrospective on Neuroimaging in AD.....   | 8    |
| 2.1 Existing Neuroimaging Databases .....  | 8    |
| 2.2 Retrospective on Multimodal Imaging for AD Classification and<br>Prediction and Measures of Caution to be Considered ..... | 9    |
| 3. Architecture of the Neuro-Imaging Web Services Interface (NWSI).....  | 17   |
| 3.1 NWSI Interface .....   | 17   |
| 3.2 NWSI Hardware Architecture.....  | 23   |
| 3.3 Image Viewer.....  | 25   |
| 3.4. Visual Rating Platform .....  | 28   |
| 3.5. SVM Classification Interface.....   | 32   |
| 3.4. Data.....   | 35   |
| 3.4.1. The 1Florida ADRC.....  | 35   |
| 3.4.2. ADNI.....   | 36   |
| 3.4.3. GAAIN (Centiloid Project).....  | 36   |
| 3.4.4. Baptist Health South Florida.....   | 37   |
| 3.4.6. SVM Classifier Data.....  | 38   |
| 3.5. Cost Analysis .....   | 39   |
| 4. Neuroimaging Capabilities.....  | 40   |
| 4.1 Volumetric and Cortical Thickness Calculations from Anatomical MRI .....   | 40   |
| 4.2 PET Imaging Analysis with 18F-Florbetapir PET / 18F- Florbetaben.....  | 41   |
| 4.3 FDG-PET in Epilepsy .....  | 46   |
| 4.4 Diffusion Tensor Imaging (DTI) .....   | 47   |
| 4.5 Data Conversion.....   | 48   |
| 4.6 The Co-Registration Tool (CRT) and Apply Matrix forms.....   | 49   |
| 4.7 Brain Extraction Tool (BET) .....  | 51   |
| 4.8 Image Display Normalization .....  | 51   |
| 4.9 White Matter Contours on PET images .....  | 53   |
| 4.10 Heat maps.....  | 55   |
| 4.11 Image Restoration .....   | 61   |
| 4.11.1 Introduction.....   | 61   |
| 4.11.2 Problems arising from Shading.....  | 65   |
| 4.11.3 Methodology for Image Restoration.....  | 66   |
| 4.11.4 Restoration and Dependence to Type of MRI Scanner .....   | 69   |
| 4.11.5 Merits of the Proposed Image Restoration Methodology .....  | 71   |
| 4.12 SVM Classification.....   | 71   |

|        |  |    |
|--------|--|----|
| 4.12.1 | Control vs. AD, RBF Kernel, corrected for ICV .....                    | 72 |
| 4.12.2 | Control vs. AD, Linear Kernel, corrected for ICV .....                 | 72 |
| 4.12.3 | Control vs. aMCI, Linear Kernel, corrected for ICV .....               | 72 |
| 4.12.4 | Control vs. AD, Linear Kernel, corrected for ICV, and using MMSE ..... | 74 |
| 5      | Validation Tests .....   | 77 |
| 5.11   | MRI Values Validation .....  | 77 |
| 5.12   | <sup>18</sup> F-Florbetapir PET Validation .....                       | 78 |
| 5.13   | <sup>18</sup> F-Florbetaben PET Validation .....                       | 78 |
| 6      | Conclusion and Future Work .....                                       | 80 |
| 6.11   | Retrospective .....  | 80 |
| 6.12   | Main Findings .....  | 80 |
| 6.13   | Future Work .....  | 86 |
|        | LIST OF REFERENCES .....   | 88 |
|        | VITA .....   | 92 |

## LIST OF TABLES

| TABLE  | PAGE |
|--|------|
| Table 3-1: Datasets Considered. ....   | 38   |
| Table 4-1: Control vs. AD, with RBF Kernel, Linear Scaling, correcting for ICV.....  | 72   |
| Table 4-2: Control vs. AD, with linear kernel, linear scaling, correcting for ICV.....   | 73   |
| Table 4-3: Control vs. aMCI, with Linear Kernel, Linear Scaling, correcting for ICV.....   | 73   |
| Table 4-4: Control vs. AD, with Linear Kernel, Linear Scaling, correcting for ICV, using MMSE. * SV: Subcortical Volumes, HS: Hippocampal Subfields, CV: Cortical volumes, TA: Thickness, SA: Surface Areas..... | 74   |
| Table 4-5: Performance average comparison of AD/Control Classification. ....   | 76   |
| Table 5-1: MRI Processing by Neuroimaging Web Services Interface (NWSI) Quality Control Comparisons. ....  | 78   |
| Table 5-2: T-Test-Paired comparing NWSI and ADNIMerge 18F-Florbetapir PET Global SUVR values.....  | 79   |
| Table 5-3: T-Test-Paired comparing NWSI and CL 18F-Florbetaben PET Global SUVR values.....   | 79   |

## LIST OF FIGURES

| FIGURE  | PAGE |
|---|------|
| Figure 3-1: MRI upload form. ....   | 19   |
| Figure 3-2: PET upload form.....  | 20   |
| Figure 3-3: DTI upload form. ....   | 21   |
| Figure 3-4: Clinical data upload form.....  | 22   |
| Figure 3-5: Field mapping. ....   | 22   |
| Figure 3-6: Virtual Architecture. ....  | 23   |
| Figure 3-7: Architecture of the NeuroImaging Web Interface System.....  | 24   |
| Figure 3-8: Interactive viewer, showing surface reconstruction and anatomical MRI...  | 26   |
| Figure 3-9: Image shows MRI, DTI and PET cross sections, ....   | 26   |
| Figure 3-10: ROI Explorer: visualizing FreeSurfer Segmentation. ....  | 27   |
| Figure 3-11: ROI Explorer: showing the left and Right Hippocampus and Amygdala...   | 28   |
| Figure 3-12: PET rating configuration form. ....  | 30   |
| Figure 3-13: Project selection as displayed to raters. ....   | 30   |
| Figure 3-14: PET rating interface and individual PET to rate. ....  | 31   |
| Figure 3-15: Classifier form.....   | 33   |
| Figure 4-1: Sample Tabulated Output for Subcortical Regions.....  | 41   |
| Figure 4-2: Page Listing PETs in the Account, with Links to the MRI used as reference.....  | 42   |
| Figure 4-3: Graph Showing the Distribution of all Uploaded 18F-Florbetapir PETs. ....   | 42   |
| Figure 4-4: Higher Concentration of 18F-Florbetapir Shown in Warmer Colors of the Spectrum Look Up Table (LUT). ....  | 43   |
| Figure 4-5: PET Image Overlaid with White Matter Surface (shown in white) and Gray Matter Surface (shown in black). The selected region's SUVR and Name are shown. ....   | 43   |
| Figure 4-6: PET Results Page Showing All SUVR Values, Links To Download Tabulated Results, and a Graph Comparing the Result to he Averages Determined in the System. .... | 44   |
| Figure 4-7: Sample Processed AD DTI. V1 Modulated by FA. ....   | 47   |
| Figure 4-8: Data Convert Tool.....  | 49   |
| Figure 4-9: Co-registration Tools: Brain Registration Form. ....  | 50   |
| Figure 4-10: PET Shown in the Papaya Viewer without Correcting.....   | 52   |

|   |    |
|---|----|
| Figure 4-11: PET Shown in the Papaya Viewer after Correcting.....   | 52 |
| Figure 4-12: Left is the PET Image without White Matter Contour, and Right Image is the Same PET with the White Matter Contour; Red Circles Indicate Areas where the Tracer has Spread to the Cortical Regions.....   | 53 |
| Figure 4-13: Full Papaya Viewer with White Matter Contour, showing SUVR Value, and Anatomical Region Name.....  | 54 |
| Figure 4-14: Heat map of Cortical and Subcortical of Right and Left Hemisphere.....   | 56 |
| Figure 4-15: Heat Map of AD (Amyloid Positive) Subject.....   | 57 |
| Figure 4-16: Heat Map of Control (Amyloid Negative) Subject.....  | 57 |
| Figure 4-17: Represents the cortical volumes. Each region was assigned the value of its volume. Regions colored with deeper shades of red have larger volumes. For this Figure a Yellow/Red color map was used instead.....   | 58 |
| Figure 4-18: Slice of a heat map Epilepsy subject showing asymmetry between homologous regions. The volume of the left temporal lobe is smaller when compared to the right.....   | 60 |
| Figure 4-19: The 3D source solution (b) is also indicating the superior temporal region as the source of the seizure; the volume asymmetry (a) is also evident in the same region.....  | 60 |
| Figure 4-20: Volume of the Superior frontal region (a) also shows asymmetry and it also coincides with some 3D results (b).....   | 61 |
| Figure 4-21: Aliasing Artifact Overlapping the Occipital Region. This Image is not Usable as the Two Signals Overlap Resulting in Erroneous Results.....  | 64 |
| Figure 4-22: Shading in the Occipital and Frontal Regions Prevent FreeSurfer from Segmenting the Image Correctly. The Blue and Red Lines Represent the White and Gray Matter Respectively.....  | 64 |
| Figure 4-23: Subject 1 Processed by FreeSurfer with Underestimated Brain Size (Shading is Indicated by the region highlighted in Green). The Blue and Red Lines Represent the White and Gray Matter, Respectively.....  | 66 |
| Figure 4-24: Extracted Brain, with visible shading in the occipital region.....   | 68 |
| Figure 4-25: Slide where the Average Values of Gray and White Matter are within 5% of the Ones Reported by FSL FAST.....  | 68 |
| Figure 4-26: Subject 1 on the left with no correction, ICV= 1277405.93 mm <sup>3</sup> . On the right Subject 1 with the corrections, ICV 1367832.66 mm <sup>3</sup> (diff=6.6%) The red and blue lines cover the whole brain volume. The blue and red lines represent the white and gray matter..... | 69 |
| Figure 4-27: Restoration dependency on Scanner Type: with older-MRI-based ICV (Model 1) being ICV: 1367832.66104 and new ICV from the more recent MRIs  |    |

(Model 2) found to be increased to 1369666.25147 (diff=1.34%) The red and blue lines are the gray and white matter. ....70

## ABBREVIATIONS AND ACRONYMS

|         |   |
|---------|---|
| HIPPA:  | Health Insurance Portability and Accountability Act |
| ICV:    | intracranial volume                                 |
| LMCI:   | Late Mild Cognitive Impairment                      |
| LONI:   | Laboratory of Neuro Imaging                         |
| MCI:    | Mild Cognitive Impairment                           |
| MPRAGE: | Magnetization-Prepared Rapid Gradient-Echo          |
| MRI:    | Magnetic Resonance Imaging                          |
| NIF:    | Neuroscience Information Framework                  |
| NIFTI:  | Neuroimaging Informatics Technology Initiative      |
| NWSI:   | Neuroimaging Web Services Interface                 |
| OHBM:   | Organization for Human Brain Mapping                |
| OS:     | Operating System                                    |
| PACS:   | Picture Archiving and Communication System          |
| PET:    | Positron Emission Tomography                        |
| PHP:    | Hypertext Preprocessor                              |
| ROI:    | Region of Interest                                  |
| RS:     | Replica Server                                      |
| SUV:    | Standardized Uptake Values                          |
| SUVR:   | Standardized Uptake Value ratio                     |
| SVM:    | Support Vector Machine                              |
| VM:     | Virtual Machine                                     |

## **1. Introduction**

### **1.1 Neuroimaging Web Services Interface and Research Significance**

This dissertation introduces a new web interface and a set of computational and machine learning algorithms to store and process neuroimaging data. Non-invasive brain imaging modalities contribute considerably to the understanding of brain structure and functionality [1]. MRI (Magnetic Resonance Imaging), Positron Emission Tomography (PET), Diffusion Tensor Imaging (DTI), and Functional Magnetic Resonance Imaging (fMRI) scans, among others, allow clinicians and experts to advance their research and take informed decisions on the diagnosis and the planning of clinical and therapeutic interventions that could follow. The images obtained by these scans must first be pre-processed in order to convert them into numeric values that can be objectively assessed and analyzed. Hospitals and other research institutions can then capture, store, and view brain scans on their own picture archiving and communication system (PACS); but performing additional processing is often computationally taxing, requiring specialized software, hardware infrastructure, and image processing expertise that our Neuroimaging Web Services Interface (NWSI) is designed to offer.

In addition to the need of individual investigators to test and validate results, there is a larger neuroscience community in hospitals, clinics and medical institutes that can benefit from this integrated processing platform. Data mining and data sharing present many challenges and opportunities to visualize and assess brain activity maps that can be viewed as a form of “neural choreography” [2]. Data sharing, which remains limited due to the different institutional and privacy constraints, should be encouraged within the

scientific community to increase the value of research. The Governing Council of the Organization for Human Brain Mapping (OHBM), the primary international organization dedicated to neuroimaging research, highlighted in 2001 certain challenges in the field of databases in neuroimaging, most of which we still face, such as (a) management of the volume and the variety of forms in which the data is presented, (b) methods for the processing of brain images, (c) accessibility of data, and (d) the lack of access to neuroimaging results to investigators [3, 4].

The proposed Neuroimaging Web Services Interface (NWSI) serves as an automated, responsive and scalable neuroimaging database solution. This new design serves also as a cyber physical system in that it offers users access to neuroimaging algorithms through the internet and provides the needed computational resources with all the required processing, storage capabilities, security and operational maintenance. It is comprised of a Web-Interface, and a set of replica Linux servers that perform specific tasks. Interacting with the system requires minimal computing knowledge, equivalent to what is expected from social media or similar type web interface [5].

NWSI is equipped with various useful tools, such as Brain Extraction Tool (BET), brain image registration, and image format conversion. The current implementation includes: (1) automatic quantification of volumes from anatomical MRIs, (2) 18F-Florbetapir and 18F-Florbetaben for Alzheimer's disease (AD), (3) FDG PET analysis for Epilepsy, and (4) DTI image processing for both AD and epilepsy. All the data results are collected in files and into a MySQL database, and can be exported into tabulated files and image files.

The accumulated data can be used in future pipelines as input to multimodal and longitudinal studies.

NWSI utilizes an embedded modified version of the Papaya viewer (a JavaScript medical research image viewer), developed by University of Texas Health Science Center. The viewer allows interactive display of cerebral regions, diffusion images, and PET data. All images are co-registered to the anatomical MRI as part of the pipeline; they can be displayed on the same viewer in stacked layers. Moreover, results have been validated by comparison to existing processed data, such as from the ADNI database, which provides an excellent source of raw and post-processed data for validating the various functions of NWSI.

NWSI has created options to display the PETs in grayscale or spectrum color schemes. It also provides a white and gray matter contour that clearly separates the gray matter from the white matter. This contour provides a more accurate way to rate the PETs as explained on chapter 4.

Neuroimaging Web Services Interface (NWSI) provides an interface to process medical images of the brain. It applies the same processing pipelines to all images of the same modality and provides the capability of performing concurrent quality control via the interface by multiple experts. The full output of FreeSurfer, including images, is provided as a download. NWSI also provides access to intermediate steps. For example, while calculating the SUVR values the regional averages are calculated before they are normalized by a region of reference. This intermediate output is also provided to the user. The transparency and options given by NWSI is not matched, to the best of our

knowledge, by any existing system. NWSI provides a system of alerts and messages that notify the user when their asynchronous processing has been completed. A help system for general usage is also provided. These complement the design of the forms that are built embedded with explanations and help on how to use NWSI. The NWSI Forum provides a space for other researchers to connect and share knowledge.

NWSI results were validated by comparing its output with data obtained from ADNI and the Centiloid Project: Global Alzheimer's Association Interactive Network (GAAIN). Both validations indicated that the difference in the data processed by NWSI and the data from GAAIN or ADNI is not statistically significant. NWSI is being actively used by researchers from multiple universities and hospitals in the US. NWSI provides the SUVR values in the centiloid scale, which allows the merging of results from different tracers (Florbetapir and Florbetaben) for PET imaging.

Image restoration is also an important issue with neuroimaging. The images are obtained from machines that create a representation of the inside of the human body. Removing noise and other artifacts is an important pre-processing step. We propose a new method to remove shading, caused by an aliasing artifact. The method corrects the images and allows the processing steps to extract accurate parameters, such as the intracranial volume (ICV) for estimating head size.

The SVM classification interface in NWSI provides the user with a simple but powerful way to conduct a variety of classification experiments on the data. Many options are selectable by the user: SMV kernel, data normalization methods, use of neurophysiological data, among others. The interface provides user-friendly interaction,

where the user does not have to be familiar with the supporting algorithms. Our Web Platform is designed for easy access to medical doctors and clinicians, who are interested in brain research, but do not necessarily, have a computer science background.

Given that the causes of AD are unknown, and a cure is not yet available, early detection is essential. When patients are cautioned that they have a possibility to develop AD, they can prepare better for the future and plan for treatment and plan early therapeutic/curative interventions. One way of detecting the possibility of AD development is to compare the patient to a population of AD, MCI, and cognitively normal (CN) individuals. Classifications algorithms, such as SVM (Support Vector machine) are suitable for such a task. Once the SVM is trained with existing data, a new data point can be placed in the context of existing subjects, and a classification into one of the prodromal stages of AD can be obtained.

## **1.2 General Statement of the Research Area**

This research seeks to provide a methodology for medical image processing through algorithms that provide results validated to current standards. The intent is to implement a web-based interface that allows 24-hour access to neuroimaging data. Users of the interface will be able to share their datasets, promoting collaboration among researchers.

## **1.3 Research Purpose**

The research aims to create a web-based multimodal neuroimaging platform. The data processed on the interface is curated and ready for discovery. NWSI provides a bridge between the image, as obtained from the scanner, and the numeric values that can be used

in classification algorithms and statistical analysis software. This is a fundamental step in the discovery process, providing researchers with results that are validated and can be trusted. NWSI creates standardized databases and allows the merging of data from different sources eliminating some of the biases that plague processing in the medical imaging realm.

#### **1.4 Significance of the Research**

Medical image processing is a field that emerged as computer hardware and software evolved. By doing a multimodal analysis of medical images researchers can learn about conditions of the brain in its normal and diseased states. NWSI addresses key issues of image registration, image processing, segmentation, image restoration, and data fusion (such as for Florbetapir and Florbetaben in PET and Centiloid scaling) and ensures correctness of the implemented algorithms through quality control and validation processes. NWSI also proposes a method to improve PET scans binary reading by using white matter contours. There is no other system, to our knowledge, capable of taking uploaded medical images and processing them into tabulated data that also provides easy sharing of information. The image restoration method proposed corrects the images and allows for accurate processing and parameter extraction.

#### **1.5 Structure of the Research**

In Chapter two, relevant research endeavors related to the research work of this dissertation are described. Chapter 3 introduces the design and architecture of the NeuroImaging Web Services Interface (NWSI). A detailed description of the system is

provided, including: (1) the hardware architecture, (2) design aspects of the interface, (3) and a cost analysis. The data from our research collaborators, including the technical details regarding its acquisition, and the number of subject for each type of scan is also provided. This Chapter also describes the design of the SMV classification form.

Chapter 4 is dedicated to research issues involving image processing, and the software pipelines embedded in the NWSI; these are addressed in Sections 4.1 through 4.7. Sections 4.8 and 4.9 discuss the advantages of automatic normalization of PET scans and the importance of white matter contour overlays in binary ratings. Section 4.10 describes a general method to create heat maps of grain regions. Chapter 4.11 describes and algorithm for medical image restoration. Section 4.12 describes a classification algorithm implemented on the web-interface Results are then presented, including many of the experiments that researchers can conduct with the interface. In Chapter 5 results derived from the system are presented, and several parts of the systems are validated by processing external data and comparing the results.

Finally, Chapter 6 concludes with a retrospective of this work together with the key findings of this research. It also outlines all the essential improvements that were made possible for the effective use of the interface and suggests future developments that could augment the proposed web interface.

## 2. Related Work and Retrospective on Neuroimaging in AD

### 2.1 Existing Neuroimaging Databases

Among the most established and widely recognized efforts to create shared neuroimaging databases is the Alzheimer's Disease Neuroimaging Initiative (ADNI) database [6], which currently contains data (some of which are longitudinal) from over 1900 subjects, encompassing over 4000 MRI and PET scans, as well as clinical, cerebrospinal fluid (CSF), genetic and biochemical biomarkers, which have been made available to researchers worldwide, who have made over 14 million downloads. Many other databases with more specialized audiences exist and have been cataloged in Neuroscience Information Framework [7]. These include: the Minimal Interval Resonance Imaging in Alzheimer's Disease database (MIRIAD) [8], the OpenfMRI database [9], NeuroVault [10], the Virtual Brain (TVB) [11], Neuroimaging Data Model (NI-MD) [12], and the Vanderbilt University Institute for Imaging Science Center for Computational Imaging (VUIIS-CCI), XNAT (Extensible Neuroimaging Archive Toolkit)-based repository [13].

The Open Access Series of Imaging Studies (OASIS), made available by the made available by the Washington University Alzheimer's Disease Research Center, Harvard University, the Neuroinformatics Research Group (NRG) at Washington University School of Medicine, and the Biomedical Informatics Research Network (BIRN), stores brain MRI data. OASIS currently contains 1098 subjects, 2118 MRI and 1500 PET images. The dataset is a retrospective compilation of collected from several ongoing

projects through the ADRC over the course of 30 years. OASIS does not allow users to upload their own images for processing.

The Collaborative Informatics and Neuroimaging Suite (COINS) [14], is a suite developed to allow data storage and sharing. The interface allows uploading the neuroimaging data, but does not provide visualization or data processing capabilities.

## **2.2 Retrospective on Multimodal Imaging for AD Classification and Prediction and Measures of Caution to be Considered**

According to the Alzheimer Association ([www.alz.org](http://www.alz.org)): Alzheimer's disease is the sixth-leading cause of death in the United States, and the only cause of death in the top 10 in the United States that cannot be prevented, cured, or slowed down, killing more than breast and prostate cancer combined. While death from other diseases has decreased significantly, from 2000 to 2013, death from Alzheimer's disease has increased by 71%. In 2015 alone, the United States will spend 226 Billion dollars to care for people with Alzheimer's. It is estimated that by 2050 the national cost could reach a trillion dollars, unless something is done to improve early diagnosis of the disease and propose new therapeutic interventions that could slow down the progression of AD. Today 5.3 million Americans live with Alzheimer's disease. Someone in the United States will develop the disease within the next 33 seconds. It is one of the factors contributing to bankrupt Medicare. AD is not simply memory loss, AD kills. In 2013, 84,000 Americans died of AD. In 2014, 15.7 million family and friends provided 17.9 billion hours of unpaid care to AD patients, valued at \$218 billion. Nearly half the population over 85 years old will

have developed AD [15]. While a cure for Alzheimer's disease will be an ideal solution, early diagnosis remains a primary requirement in prospective treatment.

Mild Cognitive Impairment (MCI) is a condition which affects the individual's abilities to perform certain thinking tasks, while the individual is still able to perform everyday activities. There are two subtypes of MCI: amnesic MCI (aMCI) and non-amnesic MCI (na-MCI). It is believed that a-MCI is actually an early stage of AD; memory loss related to the MCI subgroup, are likely to progress into AD. No single test exists to diagnose MCI in the most effective way.

Originally, AD was diagnosed without utilizing imaging or biomarkers. In 2007 the International Working Group (IWG) for New Research Criteria for the Diagnosis of Alzheimer's disease changed the basis for diagnosing AD. The new criteria also allowed diagnosing earlier stages of AD [16]. Brain Medical Imaging is a group of techniques to create visual representation of the interior of the living brain. These techniques are minimally invasive or non-invasive and allow researchers to observe the state and evolution of a diseased or healthy brain.

Brain medical images from multiple modalities as described below are obtained daily in hospitals around the world. However, not all images collected are suitable for processing. Historically doctors have looked at these images and derived visual knowledge from them, such as rating PET images by doing a binary reading. To save scanning time, some of the images are taken at low resolution (for T1 MRI images, this typically means that there are less than 64 slides per scan). The resolution of these images is so poor that they do not reveal any pertinent information when processed in a computer. Other images only

show parts of the brain and cannot be fed to the algorithms that expect a full brain in order to estimate volumes and surface areas. Amyloid PET scans are rated based on the spreading of the tracer to the cortical regions. This will show in the images as a brightening of the voxels in those areas. The gold standard is to look at these images in grayscale.

Magnetic Resonance Imaging (MRI) uses a large magnet to polarize the nuclei of hydrogen in water molecules inside the body and creates images that are representative of the anatomical features inside the brain, such as volumes and surface areas. MRI was invented in the 1970s and has proven to be very reliable in showing the anatomy of the brain. MRI allows the creation of many sequences, including but not limited to T1 and T2 weighted images (obtained by changing the relaxation time after the magnetic polarization), Fluid Attenuated Inversion Recovery (FLAIR) images (used in analyzing lesions in white matter, similar to T2 images but with much longer relaxation times), Diffusion weighted images (DWI) (used in analyzing the diffusion of water molecules in the brain, and the tracks of the neurons), and Functional MRI (fMRI), which measures brain functional activity based on the blood-oxygen-level dependent (BOLD) effect. MRI has improved since its invention, coming from 0.5 Tesla to the current 3 Tesla standard. Newer 7 Tesla scanners, with their larger signal to noise and contrast to noise ratios, create higher resolution images of the brain and will potentially allow to capture more detailed images, and introduce newer processing techniques. A special kind of DWI is the Diffusion Tensor Imaging (DTI), which maps the white matter tracks and connectivity of the brain.

Computed Tomography Scan (CT) combines X-ray measurements from different angles producing cross-sectional images of the brain. CT is typically used to detect infarcts, tumors, and calcifications, but provides less anatomical information than the MRI disciplines. Besides the X-ray based CT, other forms of CT exist, such the Positron Emission Tomography (PET), and Single-Photon Emission Computed Tomography (SPECT). PETs are of particular interest in AD research because of their capacity to measure metabolic processes. When creating a PET image, the subject is injected with a tracer that emits pairs of gamma rays indirectly emitted by the tracer. PET images are obtained with the aid of a previously obtained CT image. PETs measure blood flow in areas of high metabolic activity, capturing brighter pixels where there is more activity. They are useful in differentiating AD from other types of dementias, and localizing the focus of epilepsy seizures, among other applications in oncology and other medical disciplines.

Typical image processing pipelines involve initially processing a T1 MRI image, to obtain the anatomical data. This anatomical data contains the measurements extracted from brain structures, such as volumes of cortical and subcortical regions, surface areas of brain regions, and white matter regions. MRIs are segmented into groups of connected voxels, each representing a region. The output of processing a T1 MRI includes text files, containing the numeric measurements, and images that are registered to the T1 and represent a mapping of the brain, or specific regions of interest (ROIs). For example, in FreeSurfer the `aparc+aseg.mgz` file substitutes the intensity for each voxel by a number that represents the region a given pixel belongs to. This way, it is possible to use it as a

map of the segmented brain regions. Counting the pixels and multiplying for the voxel size provides an approximate of the region's volume. FreeSurfer defines the term "segmentation" to the partition of the subcortical cerebral regions, while calling "parcellation" to the cortical regions partition.

Given an MRI segmentation and parcellation, it is possible to register to it an image created in a different modality. PET and DTI images are diffuse and of lower resolution than MRI, they don't have enough information to be segmented by anatomical regions, but with the help of the MRI analysis it becomes possible to map a voxel from a PET image to a voxel in an anatomical region. This process also allows registering dissimilar modalities by bringing them all into the space of the T1 MRI, thus been able to display the PET and the DTI as a single registered image, allowing for the integrated analysis of assorted modalities.

Image registration, or co-registration, describes the process of aligning in space two sets of images from a same imaging modality or a set of images form two different imaging modalities. Accurate and correct image registration is essential in brain medical image analysis. Cortical brain regions make up the cerebral cortex, made entirely of gray matter; gray matter is made up of neuronal bodies. These regions form a ribbon enveloping the white matter (which contains mainly axons and extra cellular space). This ribbon is very thin, and any deviation while registering the image will produce incorrect results.

There are many software packages available with options for image registration and MRI segmentation. Among them: FreeSurfer, FSL, Mango, BrainSuite, Statistical Parametric Mapping (SPM), and 3D Slicer. The quality of the output depends largely on the quality

of the input image (including resolution, noise present in the image, contrast, and artifacts). These software packages use a combination of knowledge about the structure of the brain, combined with some sort of optimization algorithm. After the analysis is complete, a visual inspection and quality control process must ensure that the software did not make a mistake. A common error with FreeSurfer is to assume a missing region as atrophied. This causes to map regions that are not really there to white matter or other parts of the brain, producing volumetric values for areas which should have a zero-volume value.

When PETs are registered to MRI it is necessary to make sure that anatomical features visible on the PET mapped correctly to their MRI counterparts. Unfortunately, many of these software packages are based on the Linux operating system and do not provide an easy way to visualize the output. FreeSurfer provides a viewer, but in order to open it the user must use the UNIX (a family of operating systems) command line interface to load the images. This is cumbersome for many researchers and medical personnel, who have the imaging knowhow but lack the computer skills. Besides the complexity inherent to the usage of the software, these software packages require extensive computing power. FreeSurfer takes many hours to finish processing a T1 MRI on a typical server cloud environment, taking much longer in a personal computer.

Current literature also describes the difficulties of mixing imaging data from heterogenous sources. There are obvious limitations in mixing data obtained from a 1.5 Tesla scan with a 3 Tesla scan. The 3 Tesla coils produce higher quality images. A more detailed image will allow the software to better detect the edges of the regions and hence

producing more accurate structural values. But even if the intracranial volume (ICV) does not change from the 1 Tesla scan to the 3 Tesla scan, the size of regions can vary, which could misleadingly indicate a reduction or increase in size of certain regions.

Systematic artifacts and motion artifacts can bias a dataset. Younger participants in a study might have a tendency to move more than older participant, introducing artifacts that can be interpreted by the software as region size variations. Even the operator of the MRI or the scanning environment can introduce biases to the scan acquisition. Another bias may come from the processing software itself. FreeSurfer has many built-in libraries, and code created specifically by the FreeSurfer developers, but it also depends on libraries located on the host computer. That means that if there is a difference in these libraries it will be reflected on the volumetric values reported by FreeSurfer. This is known by the FreeSurfer developers, and they warn their users to not use FreeSurfer-derived data obtained from different software processing platforms in the same study. Biases sometimes will not affect the results. AD researchers look for variations in specific brain regions, such as the hippocampus, and don't look at all at other regions. But if processing bias affects one of the brain regions under scrutiny, erroneous conclusions can be drawn. Some biases may affect entire datasets.

When researchers or doctors need their images processed, they typically don't do it themselves. The images are sent to private companies or research centers. The processing facility returns the output as tabulated data rarely disclosing the processing method or providing the processed images. The researchers and doctors cannot corroborate the correctness of the output, as quality control is performed by looking at the output images,

to make sure that the algorithms performed correctly. Two sets of images might also be processed differently, introducing biases into the dataset.

When looking at the advancement of a disease and the atrophy it produces on brain regions, the changes are sometimes imperceptible. Cerebral atrophy can be severe in AD patients, but patients with subtle changes such as in MCI are more difficult to differentiate from controls. Data biased by processing can introduce changes that might be interpreted as signs of degeneration (or even regeneration) but are in reality due to the selected processing pipeline. Having a system that applies the same algorithm to all the data is key to uniformity and in solving these sorts of problems, which the NWSI is set out to achieve.

### **3. Architecture of the Neuro-Imaging Web Services Interface (NWSI)**

#### **3.1 NWSI Interface**

The web-interface driving NWSI is based on Drupal, a popular open source content management system (CMS), which is the platform for BBC, University of Oxford, the U.S. Department of Energy, and other well-established organizations. Drupal provides a user-based platform, in which the core code for the security and design tools are updated and patched frequently to address vulnerabilities, as well as to add new functionalities. New features can also be added to Drupal via modules which can be integrated with Drupal core code, allowing new code to run on Drupal, while maintaining the core software secure and intact.

The web-interface of NWSI has a simplified design, utilizing forms and uploaded files for most of the data input. Users of the interface who are not familiar with Linux or its command line arguments will be able to upload, view, or delete existing data. Figure 1 shows the MRI upload form. All data is de-identified prior to being uploaded to the server and the user determines whether or not the data on NWSI will be shared with other users. Access to the site is provided by password protected accounts. Each account represents a study, and data uploaded under that account can only be viewed by the owner of such accounts, which can be shared among members of the study.

While the user interaction occurs through the web-interface, a set of replica servers (RSs), which run on Linux, perform a variety of asynchronous tasks, such as running FreeSurfer [17] on anatomical MRIs, or registering structural MRI to PET or DTI images. To keep

the interface responsive, new tasks are sent to a work-loader on the web interface, which is based on current workload of each RS, sends tasks to one or more available RS(s). Once the data is copied back to the Web-Server, the Post-Processing Core incorporates it into the system's Database and File System. The architecture is scalable, such that new RSs, which are easy to maintain clones with identical software and capable of performing all available tasks, can be added on demand to the system.

The asynchronous communication between the web-interface and the RSs is achieved by securely copying files. Some of these files are data to be processed, while others are status reports and workload balance data. MRI, PET, DTI, and fMRI images are processed on the replica servers; but smaller tasks, such as Brain Extraction or registration, are done synchronously on the Web-Server by the Short Task Module. Tasks that are selected to run on the Small Task Modules must be brief, no longer than a few minutes in duration, so as to keep the Web-Server responsive.

The interface provides a uniform approach to all forms and data tables. For example, becoming familiar with uploading MRIs and viewing uploaded data provides insight into uploading other modalities as well. Figure 3-1 shows the MRI upload form, which contains fields for Record ID, Date, and the MRI file. Figures 3-2 and 3-3 display the PET and DTI upload pages, respectively. The PET and DTI uploads require an existing MRI to be processed. The PET upload form provides an option to upload a previously registered PET.

MRI PET DTI fMRI WMH Clinical

Processing time depends on the resolution of the MRI, and other factors, such as: how many files are in queue and servers load. Typical times are around 16-48 hours. If your MRI does is not processed in 48 hours please send us an email.

Record ID \*  
  
This field will help you find this record later.

Date  
  
E.g., 2018-02-24  
This in the date the study was performed on the patient

MRI Fields ▾

Optional Fields ▾

MRI image  
 No file selected.  
Upload a single file. If your MRI contains multiple files, zip them into a single file. Maximum file size 2 GB

Allowed formats: NIFTI, DICOM (zip files only must contain a single study and a file named: DICOMDIR) extensions: tar.gz, gz, nii, zip

Notify me when FreeSurfer Processing is complete via email  
 By clicking this checkbox you are stating that the data uploaded is de-identified \*

Figure 3-1: MRI upload form.

MRI
PET
DTI
fMRI
WMH
Clinical

This form uploads a PET and links it to an existing MRI.  
 coregisters the PET with the T1 MRI (FSL) and finds the SUV values  
 Your MRI and PET must be properly oriented to allow registration  
 Your PET must have cranium

Select Existing MRI ▼

Record ID | MRI ID | Study Date

PET image

Browse... No file selected.

Upload a PET single file. in NIFTI format (filename.nii)

PET Record ID \* ▼

This field will help you find this record later. You can enter more than 1 value separated by comas.

Date

E.g., 2018-02-24  
 This is the date the PET study was performed on the patient (This date must be as closed to the MRIs as possible)

Compound \* ▼

- Select -

The processing pipeline will be selected based on this field

Register PET before Calculations (Uncheck if PET is already registered and the **same dimensions** as the Anatomical MRI)

Registration Options ▾

Figure 3-2: PET upload form.

This form uploads a DTi for and existing MRI

Select Existing MRI

Record ID | MRI ID | Study Date

DTI Record ID \*

This field will help you find this record later. You can enter more than 1 value separated by comas.

Date

E.g., 2018-02-24

This in the date the DTI study was performed on the patient (This date must be as closed to the MRI's as possible)

B= \*

- Select -

DTI image

No file selected.

Select a DTI single file. in NIFTI format (filename.nii)

bvals

No file selected.

Select the bvals file

bvecs

No file selected.

Select the bvecs file

Figure 3-3: DTI upload form.

The Clinical form takes a CSV file with any number of rows and columns. NWSI only requires that the fields "MRI\_SITE\_ID" and "SUBJECTID" be present. Upon upload, the fields can be linked to the correct MRI record using the MRI\_SITE\_ID column. NWSI uses a number of fields to display subject information throughout the site. The user can map these fields to the ones present in the uploaded CSV. Figure 3-4 shows the clinical data upload form, and Figure 3-5 shows an example of the field mapping. The design of the clinical form allows uploading arbitrary clinical data to the interface.

MRI PET DTI fMRI WMH Clinical

Clinical Data Uploader- Uploading a file will replace (delete) all previous values. Always upload all the records. This form allows to import clinical data with any number of columns (fields) and any names, the field mapping can be done below

Current CSV FILE

CSV

Paste CSV file (headers will be used to create Database fields. Must contain: "MRI\_SITE\_ID" and "SUBJECTID", they will be used to link to the MRI Record. If you get a PDO error, you probably have columns with the same name in the CSV, rename these to have different names and try again. To upload clinical data make sure you have at least 1 MRI uploaded and completed. TODO: delete clinical file if table creation fails due to csv error...

Submit

Figure 3-4: Clinical data upload form.

Field Mapping

Select the given fields based on your field names. If fields do not exist move your option to "-Select-", if your csv fields change you must redo this mapping \*Your field names have been filter, they might look different

apoe

-Select-

-Select-

MRI\_SITE\_ID

SUBJECTID

Gender

Age

Diagnostic

SUVR\_CG

SUVR\_PONS

SUVR\_WC

SUVR\_WC\_B

SCAL\_CG

SCAL\_PONS

SCAL\_WC

SCAL\_WC\_B

race

-Select-

gender

-Select-

Figure 3-5: Field mapping.

### 3.2 NWSI Hardware Architecture

Virtual technology, VMware ESXI 5.5 with SAN (Storage area networks) and HPE MSA P2000 G3 Modular Smart Array Systems are used to host the NWSI Web-interface's and the replica servers. The cluster-aware infrastructure has two ProLiant DL 380 G7, with 2 CPUs x 3.332GHz, and 147 GB of RAM (Each), forming a centralized pool of resources that is used to create virtual machines (VMs) which run their own operating system. Figure 3-6 illustrates the virtual architecture.

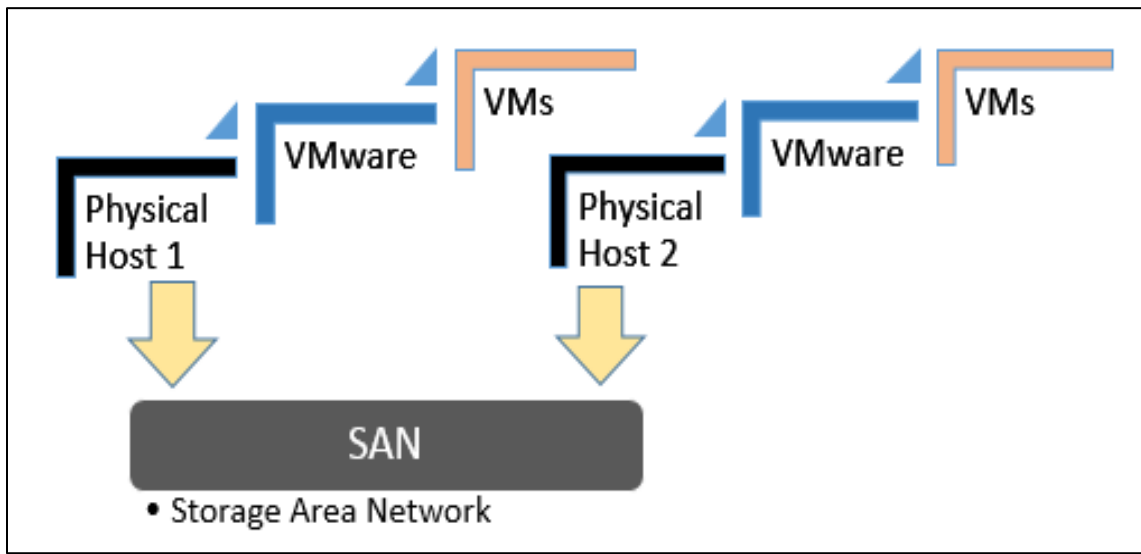


Figure 3-6: Virtual Architecture.

The Web interface runs on a Virtual Machine (VM) running Ubuntu 14.04.5 LTS (Trusty Tahr), Apache (2.4.16), PHP (5.5.28), and MySQL (5.6.26.) and is managed by Drupal 7 (latest version). The replica servers are two VMs running on Centos (6.6 el6.x86\_64.) with FreeSurfer (v5.3.0 16), each configured with 8 cores CPU and 16GB of RAM. The processing time for a single MRI is from 8 to 12 hours; however, as many as 16 MRIs can be processed simultaneously, using 2 replica servers with 8 cores each. PETs and

DTIs are processed in fifteen and ten minutes, respectively. The use of a virtual server environment adds availability, security and scalability to the Neuroimaging Web-Interface application.

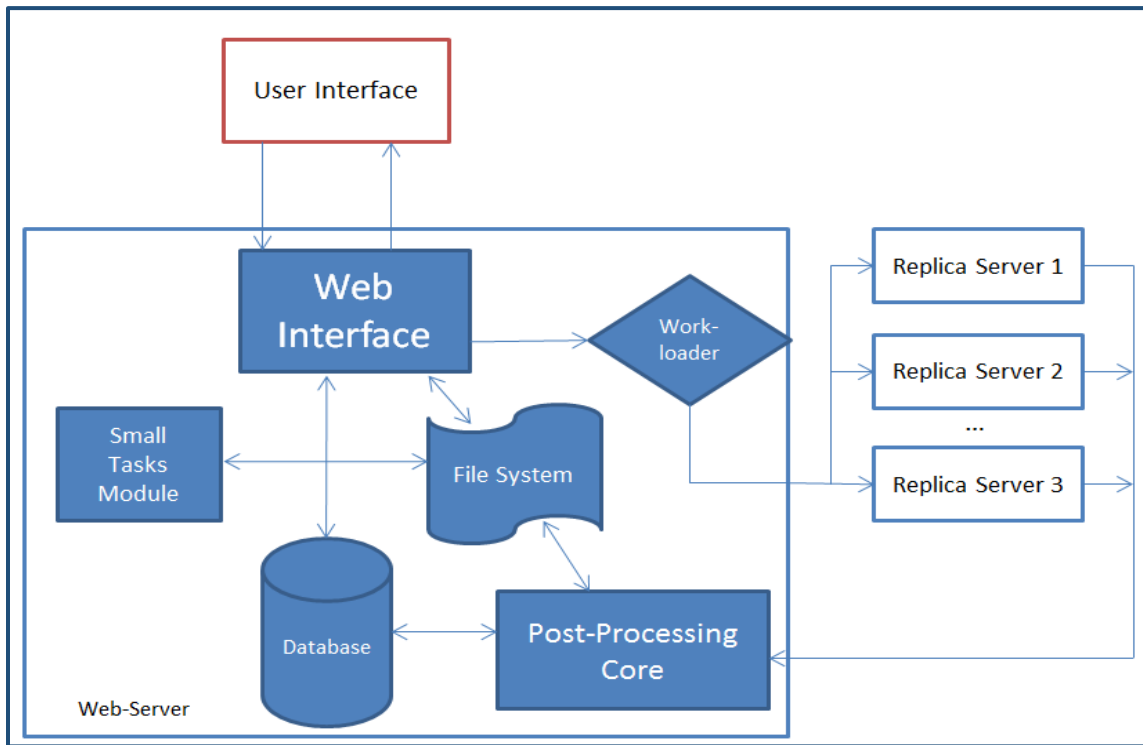


Figure 3-7: Architecture of the NeuroImaging Web Interface System.

Furthermore, new VMs can be added to the current design to increase the capability and performance of the system. Replica servers can reside in a private cloud or the Internet, as long as files can be securely copied between them and the web-interface. The web-interface can be accessed anywhere in the world with a fast Internet connection and a browser. It is both device and operating system (OS) independent. The Drupal Theme is responsive and tablet/phone friendly. Figure 3-7 above shows the architecture of the neuroimaging web-interface system, wherein the user interacts with the Web Server through the Web browser. Results from completed tasks are readily viewable. New tasks

are sent by the Work-loader, to an available Replica Server, which sends the completed task to the Post-Processing Core, from which new values are entered into the Database and raw and new images are stored on the File System. Registration, Brain Extraction, and other smaller tasks are processed on the Web-Server by the Small Tasks Module.

### **3.3 Image Viewer**

Papaya, developed by the University of Texas Health Science Center at San Antonio, is a powerful open source, interactive, JavaScript based image viewer incorporated within NWSI. The web-interface accepts the three most common medical image formats as input: single and multi-frame DICOM, ANALYZE, and NIfTI [18], but converts all files to NIfTI, which is versatile, more compact and widely used. It should be noted that some supporting software, such as FSL [19], only accepts NIfTI as input.

The version of Papaya in NWSI has been modified to display FreeSurfer labels and custom color tables. The Web Interface is also capable of displaying specific color-coded FreeSurfer regions, whole brain segmentation, interactive surfaces, PET, fMRI and DTI images. As part of our processing pipeline, all image files are registered to the structural MRI scan, making it possible to display several modalities as layers in the same viewer. Among the tools embedded on the web interface and available to the user by Papaya are color selection, a measuring tool, axis viewer, and image transparency modification, all of which are standard in many other viewers. The user can display these images online without having to save any files to the local hard disk. See Figures 3-8 and 3-9 below for illustrative examples.

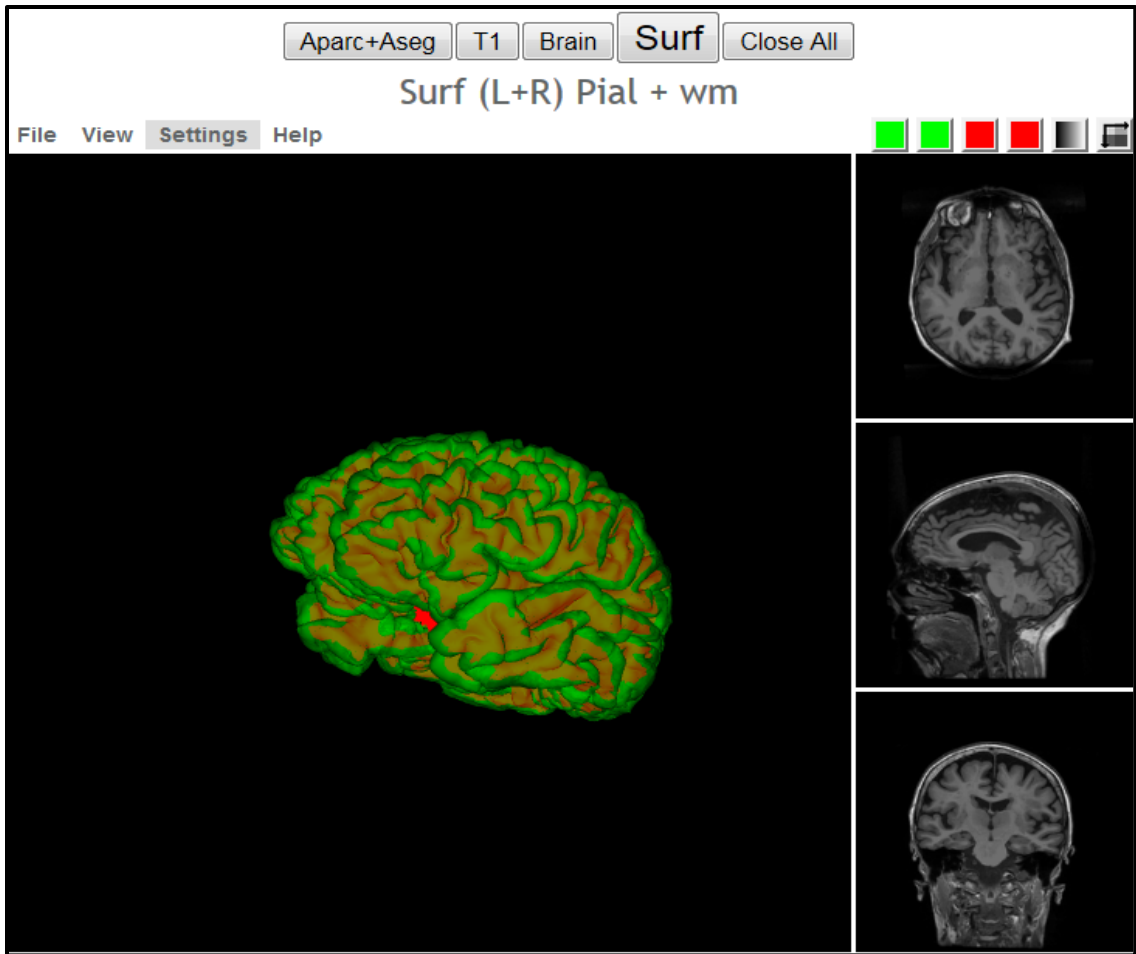


Figure 3-8: Interactive viewer, showing surface reconstruction and anatomical MRI.

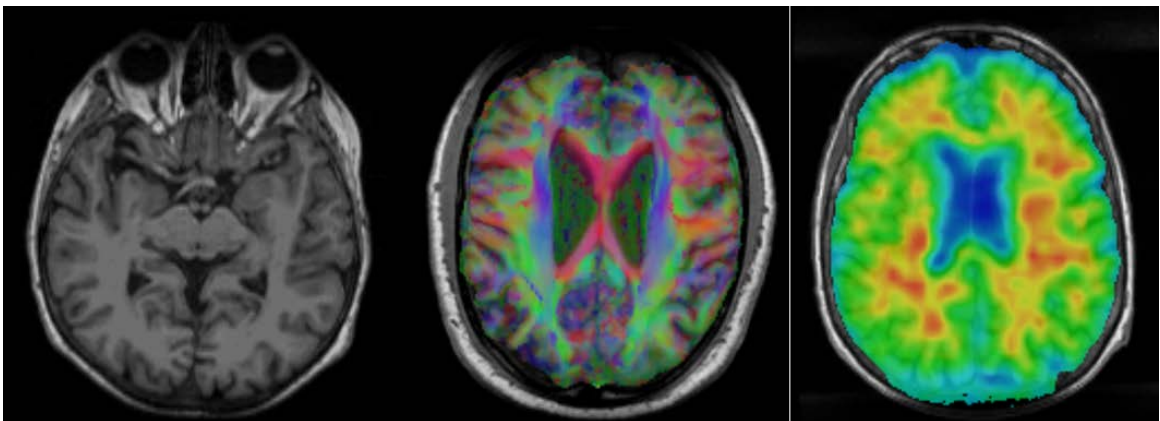


Figure 3-9: Image shows MRI, DTI and PET cross sections, as shown by the Papaya viewer.

Furthermore, the ROI explorer page displays a color-coded segmentation of FreeSurfer regions. This is especially useful for researchers who are not familiar with FreeSurfer labels but are familiar with human brain anatomy. Pertinent information can be visualized by clicking on specific regions to scrutinize what different regions reveal. See Figures 3-10 and 3-11.

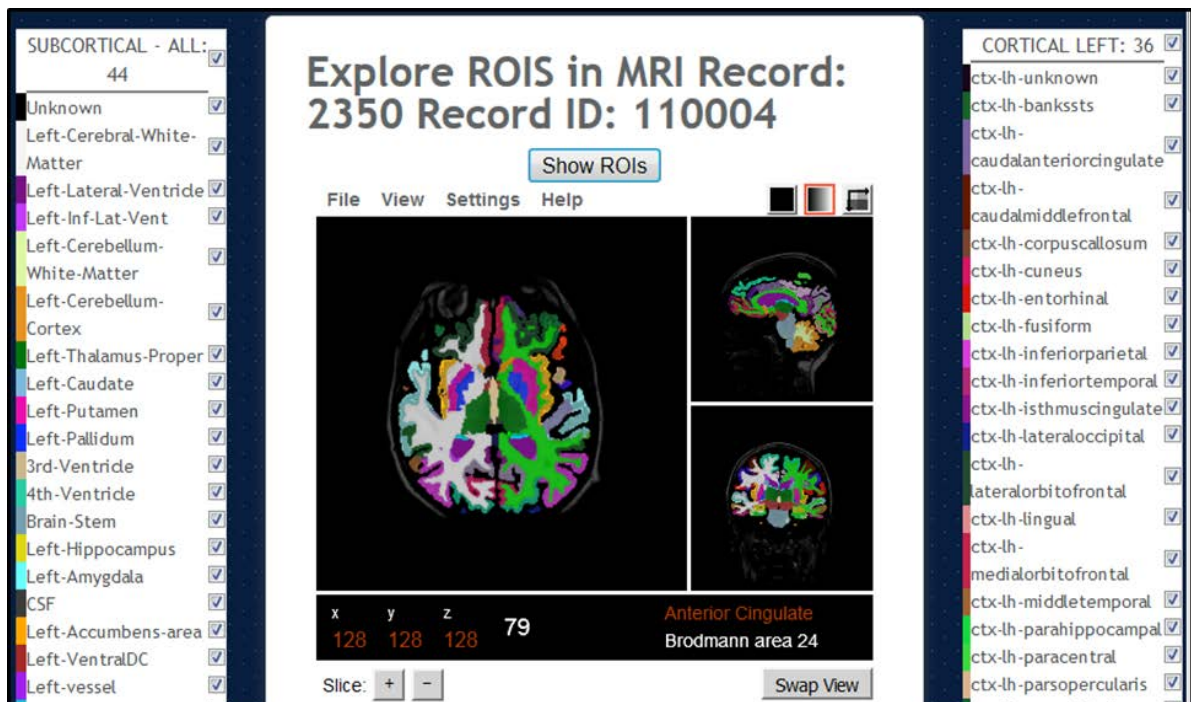


Figure 3-10: ROI Explorer: visualizing FreeSurfer Segmentation.  
By default, all regions are shown.

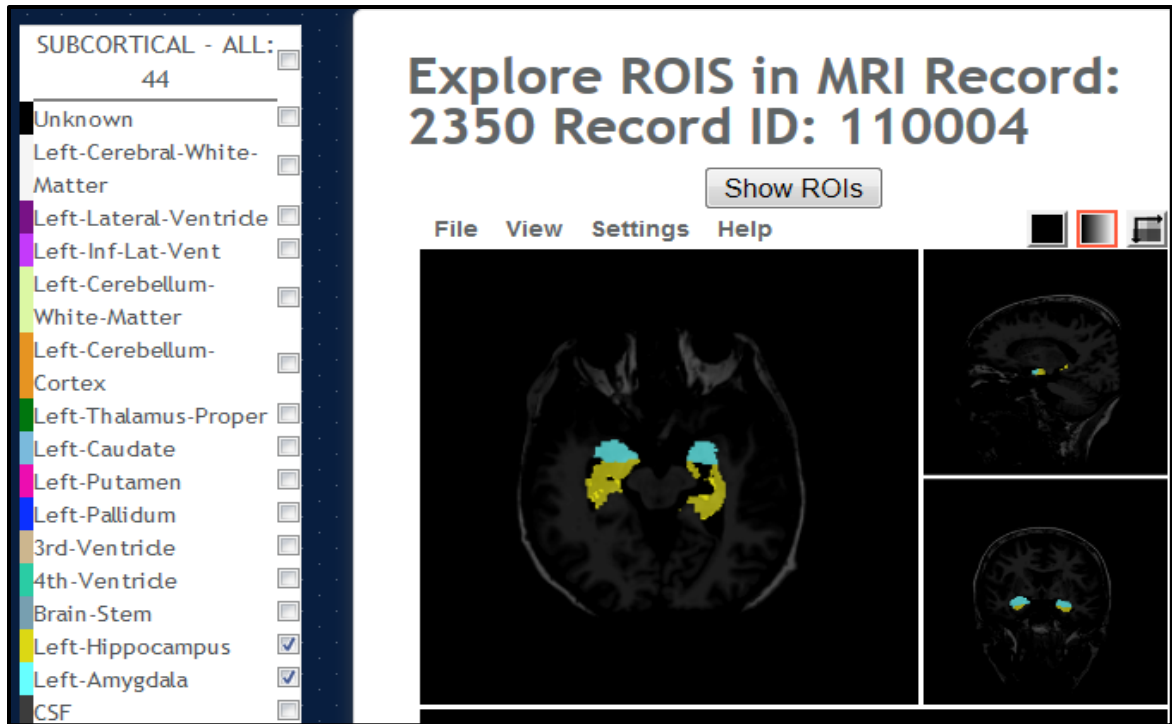


Figure 3-11: ROI Explorer: showing the left and Right Hippocampus and Amygdala.

### 3.4. Visual Rating Platform

The gold standard for Amyloid PET rating is visual ratings. Expert raters inspect the PET images and catalog them into positive, negative, or intermediate. When performing an experiment, the raters will (1) look at the PET images, (2) rate each individual image, (3) and record these values into a table. These recorded values will then have to be sent to someone who will analyze them. This process creates many issues regarding the logistic of people located in different parts of the city, or different parts of the world, looking at these images with their own viewer (not necessarily the same viewer for all raters), saving these values into a Word or Excel document, and sending the values to the processing expert. There is also the image display normalization issue, as explained in

section 4.8), where users will have to adjust the image to account for flares outside the brain within the limitations of their image viewer of choice.

NWSI provides a system to rate PETs. Images are presented to all users using the same normalization, in the same viewer, and the results are collected and stored in the same format. Furthermore, an interface was built for the processing expert to either export the data or process the data within the NWSI platform.

NWSI provides a form to create PET rating projects. These projects can be enabled or disabled, which mean whether or not they will be shown to the raters. They also contain a page size field (indicating how many PETs will be presented to the rater at each iteration), and a list of PET ids to be rated. The creator of the projects has control over how large the dataset presented to the user is. See figure 3-12.

Once a project has been created and enabled, it will show in the rater's interface. Raters can select the project and rate the images. Figures 3-13 and 3-14 show the rating interface.

if projects are enabled: rates will be able to rate once all pets 1 page size at a time. To collect new data create a new project with another name. if page count is not an integer it will default to 20 if the selection contains error the project will be disabled

**PET RATING** ▾

Projects:  ▾    Project Name:     Page Size:     Enabled:  ▾

PET Selection

Paste here you PET selection as "ADNIID-AV45-DATE". One line per subject, no repetitions. ei: 941\_S\_5193-AV45-20130627

Project Description

Describe Project

Figure 3-12: PET rating configuration form.

Projects \*

▾

Figure 3-13: Project selection as displayed to raters.



Figure 3-14: PET rating interface and individual PET to rate.

Finally, the processing expert can export the values and analyze them using a statistical software, or simply use the statistics provide by the interface. NWSI calculates the Fleiss Kappa, which is a common measure to compare ratings by multiple raters: interrater reliability. It is also possible to measure intra-rater reliability by creating projects that will be rated more than once by the same rater at different times.

### 3.5. SVM Classification Interface

The classifier, based on the libSVM (3.20) library [20], is accessible to the user as a form in the website's interface. The interface is simple yet provides many options to the user. The SVM algorithm builds a model from a set of training samples by mapping an n-dimensional array of vectors to an n-dimensional space and finding a hyperplane that separates the classes. It is a type of supervised learning, in which the training data is labeled. By default, SVM performs a linear classification, but it is possible to perform non-linear classifications by employing what is known as the "kernel trick". The SVM classification provided in the form allows selecting a linear kernel, or a Radial basis function kernel (RBF). RBF kernels at times perform better than linear kernels, but they typically don't scale well to large training samples or a large number of features. Features refer to how many dimensions the n-dimensional input space has for classification purposes, which could include structural, functional and neuropsychological measures, among others.

The form, shown in Figure 3-15, provides an option to select the classes: Control (these are subjects labeled as cognitively normal), non-amnesic MCI (naMCI: subjects with mild cognitive impairment but no memory related symptoms), amnesic MCI (aMCI: subjects with memory loss related symptoms), and AD (subjects with a diagnosis of Alzheimer's disease). Only two of the classes can be selected. Implementing an SVM algorithm with more than one class is possible but given the subtle differences in brain regional volumes that naMCI and aMCI subjects have compared to the cognitively normal group, having two classes at a time performs better than in multiclass separation

algorithms, although the advent of new machine learning algorithms could prove otherwise.

The screenshot shows a web-based classifier configuration interface. At the top, there are two tabs: "Support Vector Machine" (active) and "Neural Network". Below the tabs is the main heading "Data Mining". Underneath, there is a sub-heading "SVM Classification".

The configuration options are organized into several columns:

- Kernel Selection:** Three radio buttons are present: "Linear" (selected), "RBF", and "Kernel".
- Feature Selection:** A list of checkboxes for various features:
  - 0 Control (139)
  - 1 naMCI (220)
  - 2 aMCI (108)
  - 3 Alzheimer (76)
  - DX (select only 2)
  - SV Subcortical Volume
  - HS Hippocampus Subfield
  - CV Cortical Volume
  - TA Thickness Average (Cortical)
  - SA Surface Area
  - Correct ICV
  - Use MMSE
  - Verbose
  - Balance Data
  - Feature Selection (F-Score)
- Scaling:** Two radio buttons: "Linear" (selected) and "Scaling".
- Repetitions:** A text input field labeled "Repetitions \*" with the value "1".

At the bottom of the configuration area, there is a "Results" section with the following text:

```

SV_ Iterations: 1 Stats:
Average Sensitivity: 0.79    max: 0.79    min: 0.79
Average Specificity: 0.93   max: 0.93   min: 0.93
Average Accuracy : 0.88     max: 0.88   min: 0.88
  
```

Figure 3-15: Classifier form.

The Scaling must be selected next. Scaling makes each dimension have zero mean and unit variance. It prevents attributes with a larger range to dominate the classification as kernel values depend on the inner product of the vectors. Our method provides two types of scaling: Linear, in which the values are in the interval  $[0, 1]$ , and unit variance scaling,

in which each value is replaced by the difference from the mean, divided by the standard deviation. We found that both scaling methods work well and provide similar results.

Finally, the user must select the data features to use: the cortical volumes, hippocampal subfields, cortical volumes, thickness average, and surface areas. Each of the sets of regions is related to AD to some extent, and they are also related to each other. For example, a large regional volume will have a large surface area. We found that the hippocampal subfields (a FreeSurfer's segmentation of the hippocampus), and subcortical volumes provide a better separation of the data, as presented in the results below. Given the regions that AD typically affects, although this result was expected, it was worth validating.

Other options in the form provide additional configurations. For example, the values can be (1) corrected for intracranial volume (ICV): regional brain volumes measurements are corrected for variations in head size. (2) Use MMSE [21]: include the MMSE score in the classification, although not encouraged since MMSE is initially used at baseline, to see if the results have merits with and without inclusion of MMSE. (3) Balance data: when selecting the input select the same number vectors for both classes. (4) Feature selection: select features that are more relevant to the classification, based on their P-score. Feature selection is reported to improve the performance of classification algorithms, but we found that while other classification algorithms might be susceptible to the type of features selected, feature selection was of little effect in our SVM implementation.

### **3.4. Data**

#### **3.4.1. The 1Florida ADRC**

NWSI was piloted using a database of MRI, and amyloid PET images obtained from the Alzheimer's disease Research Center (the 1Florida ADRC). For this pilot project, currently 303 structural MRI, 45 18F-Florbetapir PET scans, and 168 18F-Florbetaben are available from the 1Florida ADRC.

MRI images were obtained using a Siemens Medical System Skyra 3 Tesla Scanner with Software version: "Syngo MR E11". Coil: "Siemens Head/Neck 20". The Scanning Sequences used was: 3D T1-W Magnetization-Prepared Rapid Gradient-Echo (MPRAGE.) Sagittal, three dimensional images with resolution of 1 mm (~12 min., TR = 2150 ms, TE = 4.38 ms, TI = 1100 ms, 160 slices, 1x1x1 mm<sup>3</sup>) obtained from approximately 1 cm left of the skull to 1 cm right of the skull, allowing room for spatial reorientation along defined anatomic coordinates.

DTI scans were obtained from the same MRI scanner. The sequence takes approximately 5 minutes (TR = 7300ms, TE = 84 ms matrix: 128x128, slice thickness =2.2 mm, number of slices = 64, iPAT factor = 2). DTI scans were used to measure radial, axial, and mean diffusivity as well as fractional anisotropy (FA).

PET images were obtained from a Siemens Biograph 16 Hi-Rez, 2006, with software version: "SYNGO CT 2009E". Image matrix 128x128, Zoom 2, Slice thickness 3.0 mm, Post reconstruction Filter: 3.0mm Gaussian. F18-Florbetapir scanning entails intravenous injection of 10mCi of tracer, a 50-minute period for tracer uptake, followed by 20-minute

scan period for image acquisition. For F18-Florbetaben imaging the dose injected was 8mCi, the uptake period between injection and image acquisition was 90 minutes and the image acquisition period was 20 minutes.

### **3.4.2. ADNI**

Data used in the preparation of this article were obtained from the Alzheimer's disease Neuroimaging Initiative (ADNI) database ([adni.loni.usc.edu](http://adni.loni.usc.edu)). The ADNI was launched in 2003 as a public-private partnership, led by Principal Investigator Michael W. Weiner, MD. The primary goal of ADNI has been to test whether serial magnetic resonance imaging (MRI), positron emission tomography (18F-Florbetapir PET), other biological markers, and clinical and neuropsychological assessment can be combined to measure the progression of mild cognitive impairment (MCI) and early Alzheimer's disease (AD).

MRI scans were acquired from 1.5T or 3T scanners at multiple sites across the United States and Canada using MP-RAGE/IR-SPGR protocols for volumetric analyses. F18-Florbetapir PET acquisition time was 50 minutes following administration of 370 MBq (10 mCi) bolus injection of F18-Florbetapir, over a 20-minute scanning period, the images were reconstructed immediately afterwards. Details of MRI and F18-Florbetapir PET imaging data acquisition are available in the ADNI website.

### **3.4.3. GAAIN (Centiloid Project)**

Data from GAAIN was made available by the researchers of the department of Molecular Imaging & Therapy in Melbourne Australia. This data was used in the Centiloid [22] project (CL). The centiloid method expresses SUVR values in a universal scale. In their

paper [23] the researchers use this data to derive the equation to convert uptake values from 18F- Florbetaben to CL values. They used 35 subjects that were scanned (MRI and 18F- Florbetaben PET): ten cognitively normal under 45 years old, and 25 AD, MCI, and frontotemporal dementia subjects. MRIs were obtained from a Siemens 3-T Trio camera with  $1 \times 1 \times 1.2$  mm voxels, and the PET scans from a Philips Allegro PET camera in 3D mode and processed with rotating Cs-137 point source attenuation correction. This data was uploaded to NWSI to validate 18F- Florbetaben SUVR calculations.

Once the SUVRs were determined, the following formulas were implemented. For Florbetaben, the centiloid formula implemented and cross-validated with [24] is:

$$CL_{units} = 153.4 \times SUVR_{Florbetaben} - 154.9 \quad (3.1)$$

On the other hand, for Florbetapir, the centiloid formula is:

$$CL_{units} = 183.07 \times SUVR_{Florbetapir} - 177.26 \quad (3.2)$$

Equation 3.2 could not be validated since they do not show the results they have obtained. All the conversion does is move a numeric value into another one, with no observable visual change, but these two formulas consolidate the scale for the images taken with these two different imaging tracers.

#### **3.4.4. Baptist Health South Florida**

Subjects from Baptist Hospital were scanned with a Philips Medical Systems, NM Division, protocol Brain Perfusion Scintigraphy. Scanning protocol: Trans AC. Slide thickness 3.195mm, Image Matrix 128x128. Contrast: FDG – fluorodeoxyglucose.

### 3.4.5. Nicklaus Children's Hospital

Subjects from Nicklaus Children's Hospital were scanned with a GE Medical Systems, model: Discovery ST. Scanning protocol: PET AC 3D Brain. Slide thickness 3.27mm, Image Matrix 128x128. Contrast: FDG – fluorodeoxyglucose.

### 3.4.6. SVM Classifier Data

The classifier was linked to ADNI Data. ADNI provides a dataset for AD research. The input features were selected from the ADNIMERGE document, available for download on the LONI site. We also tested the algorithm with data from the Wien Center for Alzheimer's Disease and Memory Disorders at Mount Sinai Medical Center, Miami Beach. Our datasets are as described in Table 3-1. Volumetric measurements in ADNI data were obtained using FreeSurfer 5.1, processing the MP-RAGE protocol sequence, with 1.5 Tesla scanners. The

Wein Center data was obtained from T1 weighted MP-RAGE scans, from a Skyra 3 Tesla scanner. The results were processed in FreeSurfer 5.3 at the Center for Advanced Technology and Education (CATE), Florida International University. All subjects went through similar visual quality control processes.

Table 3-1: Datasets Considered.

| Class  | ADNI         | Wien Center  |
|--------|--------------|--------------|
| Normal | 139 subjects | 127 subjects |
| Na-MCI | 220 subjects | 55 subjects  |
| a-MCI  | 108 subjects | 68 subjects  |
| AD     | 76 subjects  | 61 subjects  |

### **3.5. Cost Analysis**

NWSI scalability allows for a large number of additional replica servers. The basic requirement is two servers: one hosting the web interface, and the other for processing images. This setup was the initial prototype and it worked well for small batches of less than 20 or 30 sets all uploaded at the same time. The cost of maintaining two dedicated servers is low: services such as Godaddy.com provide each server from \$69.99 per month for a dedicated Linux server. The current prototype is installed on a distributed system located at Florida International University. This type of setup is more secure and easier to manage, having a larger price tag. FIU paid \$62,000.00 including hardware and software licenses. If all the resources are utilized the FIU setup can service many requests, with the capability to process hundreds of MRIs and PETs per day. The prototype only uses 3 servers from up to 15 servers which can be created on this distributed system with 8 cores and 32GB each.

## 4. Neuroimaging Capabilities

### 4.1 Volumetric and Cortical Thickness Calculations from Anatomical MRI

The basic functionality of NWSI depends on using FreeSurfer to reconstruct cortical surface models (gray-white boundary surface and pial surface) from structural MRIs and to output regional cortical and subcortical volumes, cortical thickness, and other values derived from input image segmentation (see FreeSurferWiki (fswiki) for a complete list of such measures). FreeSurfer also outputs image files that define the segmentation and replaces intensity on these files by numeric values representing the segmented regions. These files are used in the calculation of PET Standardized Uptake Values (SUV).

NWSI processes all structural MRIs on a local server, rather than using the option of uploading existing FreeSurfer values, because it was determined on testing the system that FreeSurfer results were affected by the OS version adopted, even when the same FreeSurfer version was used [25]. This outcome serves as a measure of caution, especially for comparative studies and analyses. FreeSurfer specifies in the fswiki that when processing a group of subjects, it is essential to use the same FreeSurfer version on the same OS platform and vendor, because certain OS level libraries might affect the results. As new replica servers are added to the system, it is imperative to test them before deployment to make sure the results are validated against established ones.

An important issue, which can be resolved by NWSI, is the merging of data from different sources, which is a non-trivial task due to factors such as scanner bias, scanner field strength, among others [26]. This problem is best addressed by processing all values

with the same hardware and software, once enough data from different sources is present on the server. Results from subjects from one institution (e.g., control subjects) can be merged with subjects from another institution, downloaded and tabulated in a format. Figure 4-1 shows a sample comma separated values output.

| A         | B         | C            | D            | E          | F          | G          | H         | I          | J           | K         |
|-----------|-----------|--------------|--------------|------------|------------|------------|-----------|------------|-------------|-----------|
| Record ID | Measure   | Left-Lateral | Left-Inf-Lat | Left-Cereb | Left-Cereb | Left-Thala | Left-Caud | Left-Putar | Left-Pallic | 3rd-Ventr |
| 110025    | 215_-1_-1 | 23778.1      | 270.1        | 15368.7    | 46407.1    | 8106.9     | 3553.8    | 5825       | 1846.8      | 2399.4    |
| 110026    | 215_-1_-1 | 13807        | 438.2        | 13988.8    | 40207.9    | 6105.2     | 2989.4    | 4500.6     | 1247.8      | 1457.6    |
| 110033    | 215_-1_-1 | 35533.9      | 3090         | 17376.9    | 47329      | 10878.9    | 2276.5    | 2338.3     | 1200.8      | 3712.1    |
| 110034    | 215_-1_-1 | 37264.6      | 2386         | 4892       | 26241.9    | 8561.6     | 2182.4    | 2212.5     | 3297.1      | 2092.7    |
| 110038    | 215_-1_-1 | 14027.4      | 574.6        | 12256.4    | 49011.8    | 7930.9     | 3419.2    | 4142       | 1171.9      | 1442.2    |
| 110041    | 215_-1_-1 | 20431.8      | 540.6        | 14090.2    | 38588.9    | 7531.5     | 2152.3    | 3818       | 1174.4      | 1700.2    |
| 110042    | 215_-1_-1 | 10929.7      | 531.8        | 18459.8    | 55887.7    | 8679.8     | 3367.1    | 4289.7     | 1097.4      | 1462.2    |
| 110044    | 215_-1_-1 | 16508.6      | 455.8        | 16232.2    | 40618.9    | 8765.5     | 3502.6    | 3893.9     | 1031.6      | 1038.5    |

Figure 4-1: Sample Tabulated Output for Subcortical Regions.

#### 4.2 PET Imaging Analysis with 18F-Florbetapir PET / 18F- Florbetaben

Regional quantification of regions of interest (ROI) is still defined manually, but automatic Standardized Uptake Value ratio (SUVR) calculations and segmentation of PET images have become the gold standard [4]. NWSI implements several PET analysis pipelines for FDG and 18F-Florbetapir images. Prior to uploading a PET scan, a structural MRI must already exist in the system; the user is presented with a form in which an existing MRI must be selected. After the PET scan is uploaded, it is copied to one of the RSs for processing and can be accessed through a form that lists all uploaded records, as shown in figure 4-2. This form also contains graphs showing the distribution

of all PET scans uploaded by the user as in Figure 4-3. Once a PET scan is processed, it can be displayed on the interactive image viewer, as shown in Figure 4-4 and Figure 4-5, and then quantitative data can be downloaded from the PET scan page, as shown in Figure 4-6.

**View PETs**

Search Record ID  
  
 Enter Record IDs separated by spaces Apply

| ID   | RECORD ID | STUDY DATE | UPLOADED FILE            | COMP   | SUVR | STATUS    | MRI                 | PET                 | EXPLORE                 | EDIT                   |
|------|-----------|------------|--------------------------|--------|------|-----------|---------------------|---------------------|-------------------------|------------------------|
| 2404 | 110004    | 2015/05/25 | <a href="#">Download</a> | Amyvid | 1.08 | completed | <a href="#">MRI</a> | <a href="#">PET</a> | <a href="#">explore</a> | <a href="#">Delete</a> |
| 2405 | 110007    | 2015/06/06 | <a href="#">Download</a> | Amyvid | 1.22 | completed | <a href="#">MRI</a> | <a href="#">PET</a> | <a href="#">explore</a> | <a href="#">Delete</a> |
| 2406 | 110008    | 2014/08/13 | <a href="#">Download</a> | Amyvid | 1.03 | completed | <a href="#">MRI</a> | <a href="#">PET</a> | <a href="#">explore</a> | <a href="#">Delete</a> |
| 2407 | 110009    | 2015/06/16 | <a href="#">Download</a> | Amyvid | 1.08 | completed | <a href="#">MRI</a> | <a href="#">PET</a> | <a href="#">explore</a> | <a href="#">Delete</a> |
| 2408 | 110011    | 2015/06/30 | <a href="#">Download</a> | Amyvid | 1.13 | completed | <a href="#">MRI</a> | <a href="#">PET</a> | <a href="#">explore</a> | <a href="#">Delete</a> |
| 2409 | 110012    | 2015/06/30 | <a href="#">Download</a> | Amyvid | 1.06 | completed | <a href="#">MRI</a> | <a href="#">PET</a> | <a href="#">explore</a> | <a href="#">Delete</a> |

Figure 4-2: Page Listing PETs in the Account, with Links to the MRI used as reference.

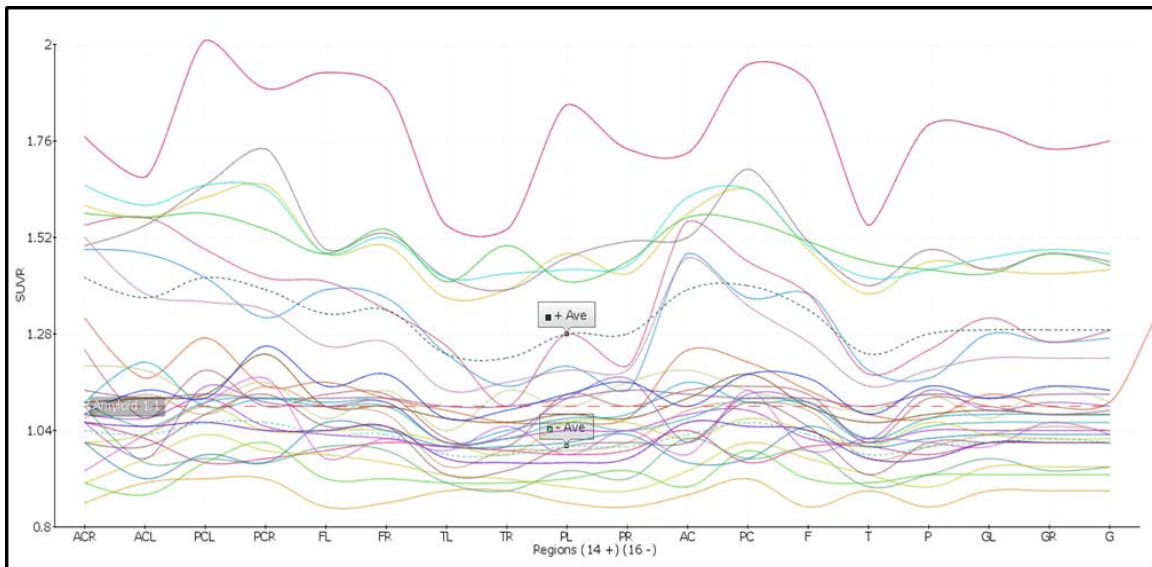


Figure 4-3: Graph Showing the Distribution of all Uploaded 18F-Florbetapir PETs.

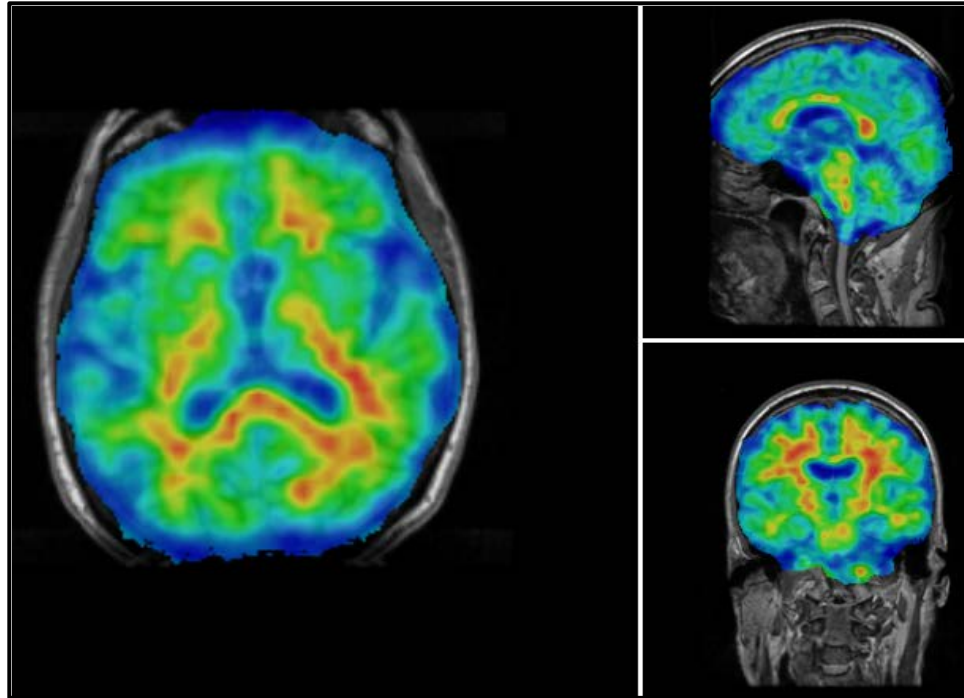


Figure 4-4: Higher Concentration of  $^{18}\text{F}$ -Florbetapir Shown in Warmer Colors of the Spectrum Look Up Table (LUT).

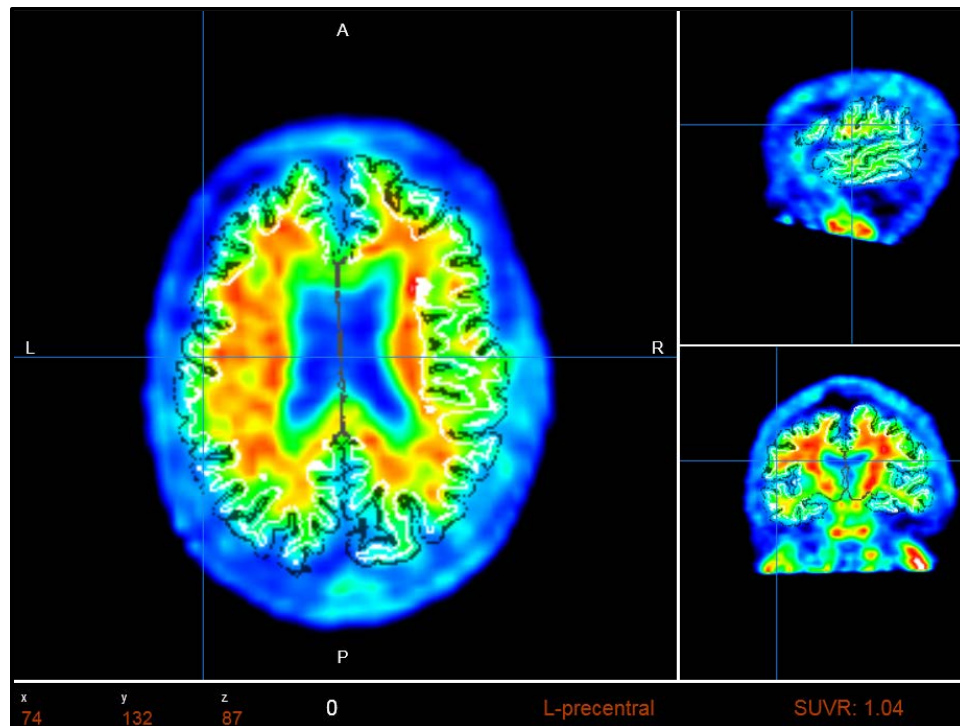


Figure 4-5: PET Image Overlaid with White Matter Surface (shown in white) and Gray Matter Surface (shown in black). The selected region's SUVR and Name are shown.

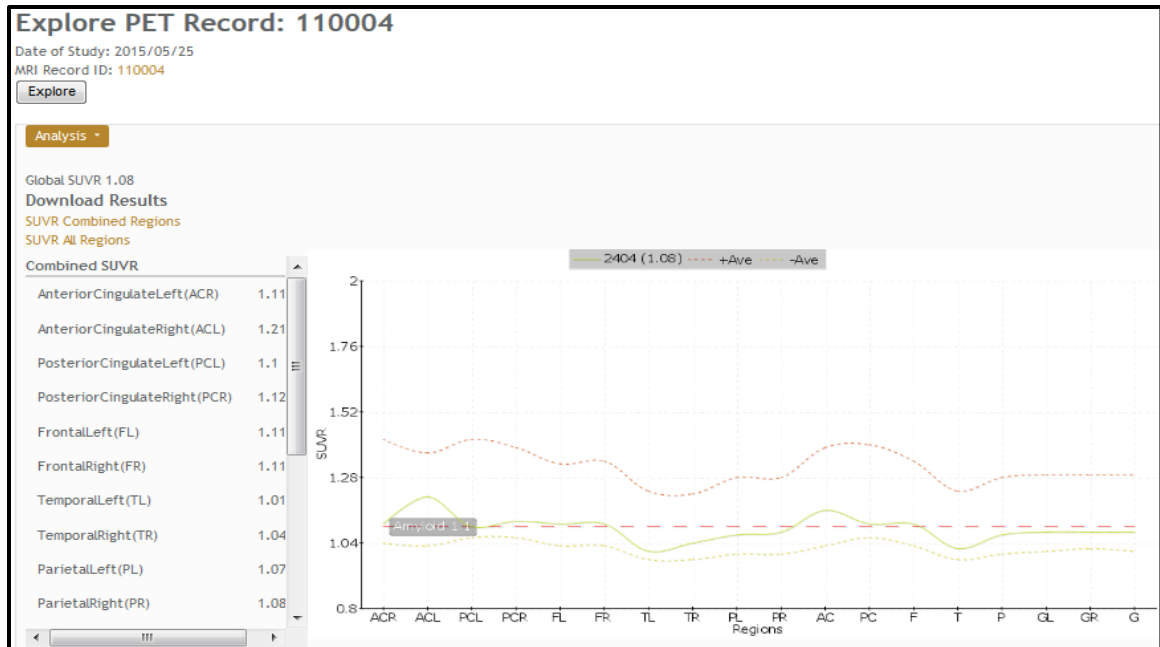


Figure 4-6: PET Results Page Showing All SUVR Values, Links To Download Tabulated Results, and a Graph Comparing the Result to he Averages Determined in the System.

It is essential that the PET image is co-registered to the anatomical MRI because all calculations depend on how closely the anatomical regions of the two images overlap. A particular challenge for aging and AD and other neurodegenerative diseases is atrophy correction. It should be indicated that co-registration to MRI images largely reduces artifacts related to atrophy. The current implementation aligns the images using FSL. The alignment uses 12 degrees of freedom (3 translations, 3 rotations, 3 scalings, and 3 Skews/Shears). Then, a so-called custom R software opens the co-registered PET and the FreeSurfer segmentation volume, performing a voxel by voxel analysis of the intensities of the PET file, and accumulating values per anatomical ROI. The average over a region provides the SUVs, as given in Equation (1). The SUVR are then calculated by dividing the SUV by a region of reference (SUVRG) as expressed in Equation 2. Larger regions, aggregated from FreeSurfer sub-regions can also be calculated. SUVR, for combined

FreeSurfer regions (CB), are calculated by a volume weighted average of previously calculated SUVR as described by Equation 3.

$$SUV_{ROI_i} = \frac{\sum_{k=1}^{N_{ROI_i}} Intensity_k}{N_{ROI_i}} \quad (4.1)$$

Where  $N_{ROI_i}$  is the total number of voxels in  $ROI_i$ ,  $Intensity_k$  is the value of voxel k in  $ROI_i$  in PET image.

$$SUVR_{ROI_i} = \frac{SUV_{ROI_i}}{SUV_{RG}} \quad (4.2)$$

$$SUVR_{CB} = \frac{\sum_{i=1}^m SUVR_{ROI_i} \times V_{ROI_i}}{\sum_{i=1}^m V_{ROI_i}} \quad (4.3)$$

Where the CB consists of  $m$  ROIs,  $SUVR_{ROI_i}$  and  $V_{ROI_i}$  are the corresponding SUVR and volume of ROI sub-regions, respectively.

Current literature mentions the merits of using an assortment of reference regions, such as the total or eroded subcortical white matter, the brain stem, the whole cerebellum, or the cerebellar white matter [27]. SUVR results, normalized by the whole cerebellum, have been validated using values reported by ADNI. NWSI also calculates SUVR using unilateral or bilateral cerebellar white matter. The values can be exported on tabulated files.

PET imaging with 18F-Florbetaben also measures global cortical amyloid load and uses a similar processing pipeline to 18F-Florbetapir images. However, statistics and results on

NWSI are reported separately to avoid bias. Studies have shown that there are no marked differences in the diagnostic accuracy of the amyloid binding ligand [28].

### **4.3 FDG-PET in Epilepsy**

PET imaging using Fluorodeoxyglucose (FDG), labeled with a positron emitting tracer [Fluorine-18], or FDG-PET, is used to measure regional glucose metabolism, which is strongly correlated to, and widely used to measure regional neuronal activity in the brain [29]. To study epileptic conditions using FDG-PET, in combination with structural MRI, regional SUVR is calculated using the cerebellar white matter, or the whole cerebellum, as a reference region [30]. In studying epilepsy, special consideration needs to be given to identifying focal conditions in one hemisphere and to account for surgical resection of regions in the brain. The FDG-PET pipeline in NWSI allows a choice of several reference regions, including the whole cerebellum, the cerebellar white matter, the average of all bilateral cortical regions (global cortical SUV), or all regions for a single intact hemisphere (in subjects who have had a prior resection in one hemisphere).

The PET images are superimposed on MRI brain scans for defining the underlying structure and brain regions which have been resected. Regional SUVR is derived similar to the procedure for amyloid PET scans, and asymmetry in corresponding bilateral regions is calculated by dividing the difference in SUVR among corresponding bilateral regions by their sum and multiplying by 100%, as shown in Equation 4. Reference regions are not required in this calculation of asymmetry; a difference of 10% or greater between bilateral regions is typically considered to be consequential.

$$Dif_{ROI_i} = \frac{SUVR_{ROI_i}^L - SUVR_{ROI_i}^R}{SUVR_{ROI_i}^L + SUVR_{ROI_i}^R} \times 100\% \quad (4.4)$$

$SUVR_{ROI_i}^L$  and  $SUVR_{ROI_i}^R$  are the SUVR of  $ROI_i$  in the left and right hemisphere.

#### 4.4 Diffusion Tensor Imaging (DTI)

DTI analysis on NWSI is still under development. Currently, the DTI is obtained by executing the DTIFit FSL tools on an anatomically co-registered Diffusion-Weighted Image (DWI) that has been corrected for Eddy currents. The DTIFit program fits a diffusion tensor model at each voxel. The resulting DTI eigenvalues and eigenvectors can be shown on the web interface viewer modulated by the Fractional Anisotropy (FA) image. As these images are co-registered to the anatomical MRI, further analysis can be done to obtain numeric values for anatomical ROIs. See Figure 4.7.

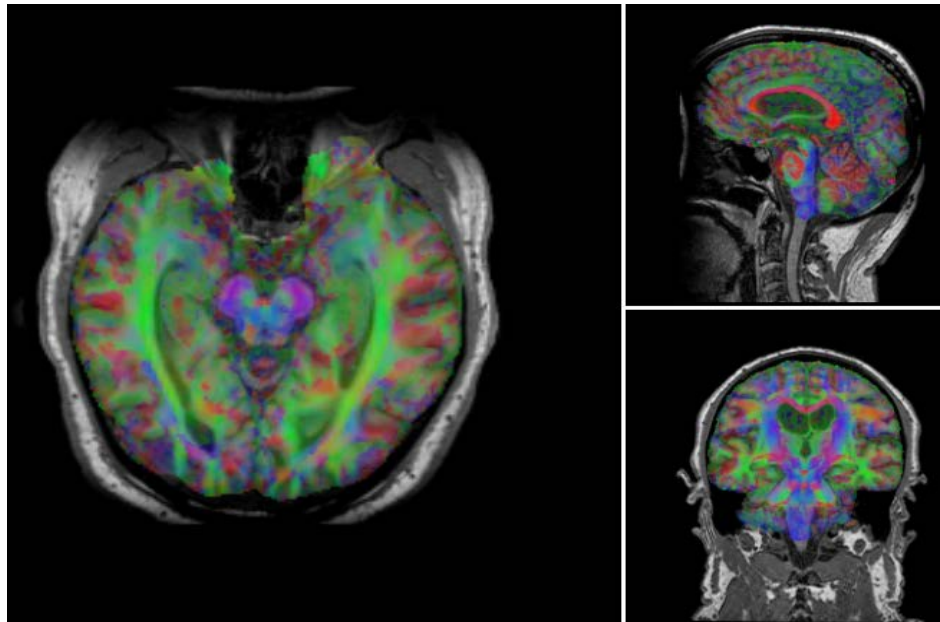


Figure 4-7: Sample Processed AD DTI. V1 Modulated by FA. Colors Represents Direction of Water Movement: Green is front to back. Blue is head to foot. Red is left to right.

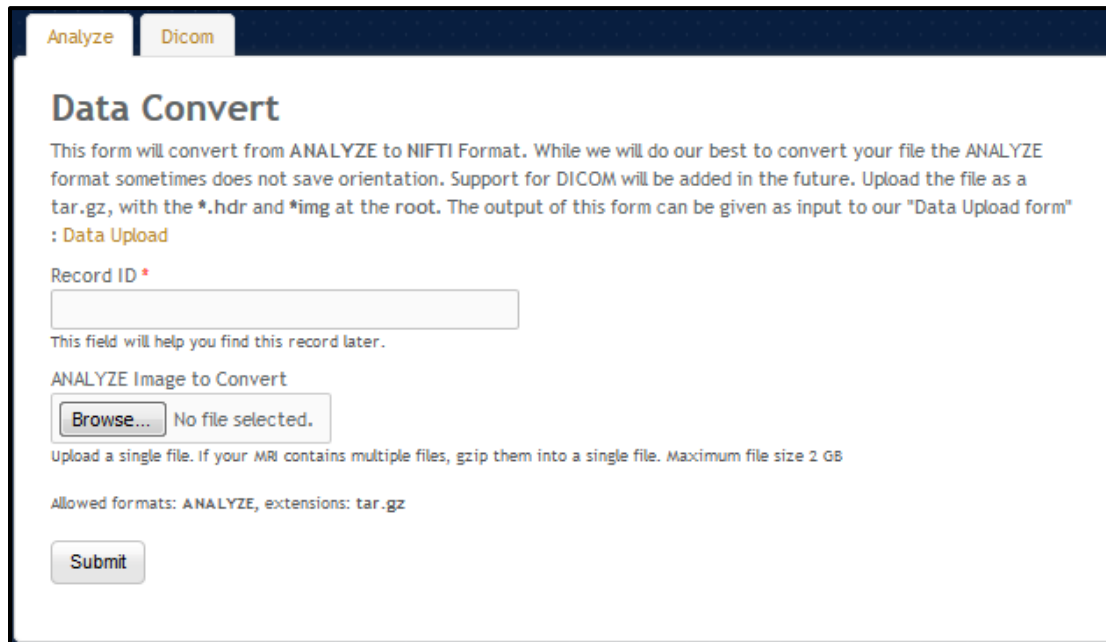
## 4.5 Data Conversion

There are currently three main image formats for storing medical images. Digital Imaging and Communications in Medicine (DICOM), ANALYZE, and Neuroimaging Informatics Technology Initiative (NIFTI). The DICOM format was introduced in the 1980s, and has gone through several revisions since, to arrive at the current standard. It is the preferred format scanners use to save or store images.

NWSI can take DICOM as input in several of the forms. The ANALYZE format (also known as ANALYZE 7.5) was created by the Mayo Clinic as the default format for their Analyze software. The ANALYZE format lacks consistency regarding orientation of the image, making it unsuitable for research. NWSI provides support to convert from ANALYZE to NIFTI. The NIFTI format, introduced in 2003, which was developed to replace the ANALYZE format, is the preferred format among researchers. It addresses the issue of spatial orientation. NWSI uses predominantly the NIFTI format because it makes forms simpler and uploads consist of a single file.

The Data Convert (DC) form contains two menu tabs, each indicating either ANALYZE or DICOM, and contains fields for uploading a file and recording ID. Upon submitting the form, the file is converted and saved in the file system in NIFTI format and is stored in the Converted MySQL table. The converted file can be downloaded by the user immediately after conversion, or anytime later. The Conversion algorithms call functions in FreeSurfer and FSL, depending on the input. It also decompresses the image file, if it were compressed. Compression is used to save storage space, but many software packages like FreeSurfer do not take compressed DICOMs as input. The DC tool

produces a standardized NIFTI file that can serve as input to most processing software, including FreeSurfer, SMP8, and FSL. See Figure 4-8 for a screenshot of the Data Convert form.



The screenshot shows a web interface for a 'Data Convert' tool. At the top, there are two tabs: 'Analyze' (selected) and 'Dicom'. The main heading is 'Data Convert'. Below the heading is a paragraph of text explaining the tool's purpose: 'This form will convert from ANALYZE to NIFTI Format. While we will do our best to convert your file the ANALYZE format sometimes does not save orientation. Support for DICOM will be added in the future. Upload the file as a tar.gz, with the \*.hdr and \*img at the root. The output of this form can be given as input to our "Data Upload form" : Data Upload'. Below this text is a text input field labeled 'Record ID \*' with a placeholder box. Underneath the field is a note: 'This field will help you find this record later.' The next section is 'ANALYZE Image to Convert', which contains a file selection button labeled 'Browse...' and the text 'No file selected.'. Below this is a note: 'Upload a single file. If your MRI contains multiple files, gzip them into a single file. Maximum file size 2 GB'. The next line says 'Allowed formats: ANALYZE, extensions: tar.gz'. At the bottom of the form is a 'Submit' button.

Figure 4-8: Data Convert Tool.

#### 4.6 The Co-Registration Tool (CRT) and Apply Matrix forms

The CRT Tool allows co-registering one brain image to another, from similar or different modalities. This form uses FSL tools to align the images and exports many of the options to the user, such as: (a) extract the brain from source images before registration, and (b) define the degrees of freedom, cost function, or angle to rotate the images. For most of the AD data processed in NWSI, default FSL registration parameters work well. However, some images have noise or artifacts and cannot be used for automatic registration. CRT allows the user to find the registration parameters for individual images before they are uploaded to other processing pipelines. Current and previous results can be inspected in

an embedded viewer. Co-registration is the main step to many processing pipelines, especially for multimodal imaging. Many algorithms, calculating multimodal values, depend on a perfect registration (overlay) of both images. Figure 4-9 shows the CRT form.

The Apply Matrix Tool applies an existing FSL matrix transformation to an image. A matrix transformation is defined within FSL as the transformation parameters. It is a text file which saves the 12 transformation parameters applied in the registration process: rotation, scaling, skew, and origin (3 coordinated for each).

The screenshot shows a web-based form titled "Brain Registration Form" with three tabs: "Registration", "Apply Matrix", and "BET". The "Registration" tab is active. The form contains the following elements:

- Header:** "This form allows the registration of two single volume brain images"
- Input Image:** A "Browse..." button and the text "No file selected." Below it, a note: "Upload file in nii.gz format. Image should be single volume"
- Color Table:** A dropdown menu set to "Spectrum" with the label "Color Table for input file"
- Reference (typically a T1 anatomical Image):** A "Browse..." button and the text "No file selected." Below it, a note: "Upload file in nii.gz format"
- Color Table:** A dropdown menu set to "Grayscale" with the label "Color Table for reference file"
- Checkboxes:** Two checked checkboxes: "Extract **Input** image Brain (BET) before registration." and "Extract **Reference** image Brain (BET) before registration." Below these is a note: "if only 1 option selected above, the other images must be an extracted brain"
- BET input f:** A text input field containing "0.5" with a note: "Input image Brain Extraction 'f' parameter (higher numbers remove more skull.) Numeric values between 0->1"
- BET ref f:** A text input field containing "0.5" with a note: "Reference image Brain Extraction 'f' parameter (higher numbers remove more skull.) Numeric values between 0->1"
- Final Checkbox:** A checked checkbox: "Transform Reference to **Standard Space**. Removes the neck of reference image"

Figure 4-9: Co-registration Tools: Brain Registration Form.

#### **4.7 Brain Extraction Tool (BET)**

The BET tool interfaces with FSL to extract the brain in a medical image. All command line options are exported to the interface. Extracting the brain is the first step in many processing pipelines. Images that were cropped at scanning time cannot be registered to complete images because the complete images have extra information that cannot be matched. During the registration process, it is sometimes required to extract the brain from both images, to later apply this registration matrix for the whole image to be registered.

#### **4.8 Image Display Normalization**

NWSI provides several views of the same data. MRI results contain the ROI explorer, the Segmentation, T1, Brain, and a surfer viewer. These images come from FreeSurfer, and the voxel values are normalized between 0 and 255 for an 8-bit resolution. NWSI leaves PETs in their original resolution because normalizing the values will impact the SUVR calculations. PET images sometimes contain very high voxel values in non-brain areas. These higher values skew the range of the intensity values and lower the contrast within the brain. Figure 4-10 shows a sample PET with these flares of brightness around the neck.

These brighter areas are unimportant and play no role in the calculation of SUVR values. NWSI uses the maximum and minimum value within the brain to normalize the PET image at display time. The new image, as shown in Figure 4-11, discerns the gradient of amyloid deposition in the brain much better. This normalization is done automatically.

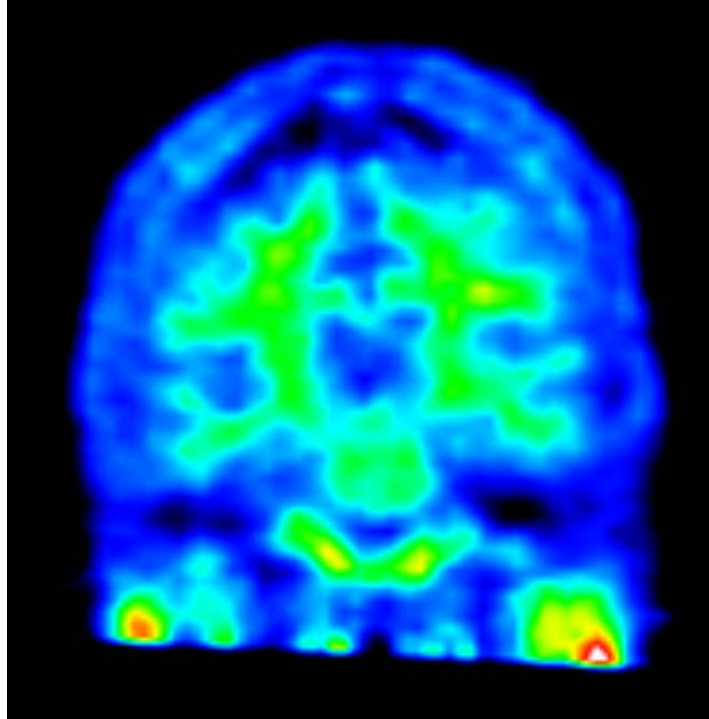


Figure 4-10: PET Shown in the Papaya Viewer without Correcting for extrema values Inside the Brain.

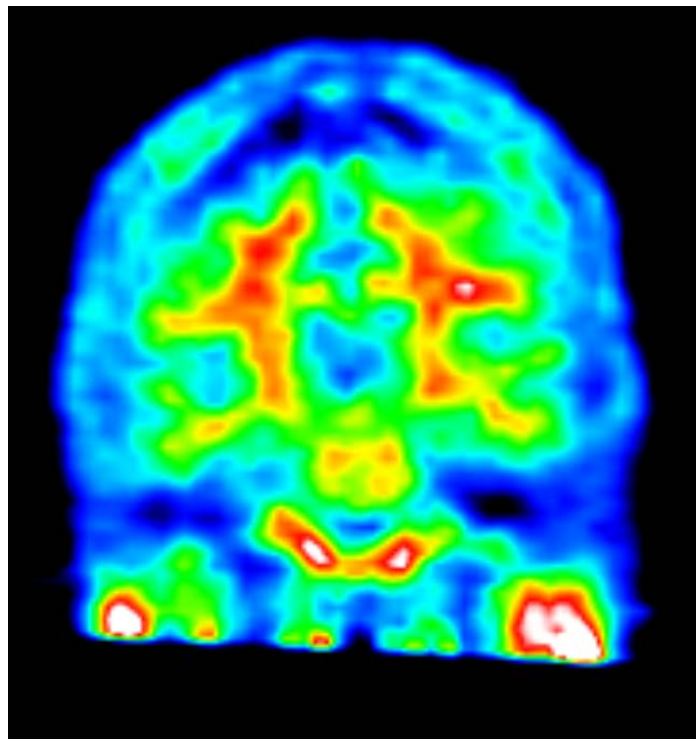


Figure 4-11: PET Shown in the Papaya Viewer after Correcting for Extrema Values Inside the Brain.

#### 4.9 White Matter Contours on PET images

Another contribution of the NWSI web interface is in utilizing white matter contours to aid in PET visual ratings. The gold standard for visually rating PETs is to display them in grayscale and visually assessing how much brighter are the cortical regions in contrast to white matter. The problem with that process is that it requires knowledge of the anatomy of the brain, and keen visual perception gained through years of experience of the visual rater. Figure 4-12 (right) shows a sample PET with the white matter contour. The red circles mark regions where the tracer has spread to cortical regions. Without the white matter contour, it will be really difficult to rate this PET without an understanding of the brain anatomy.

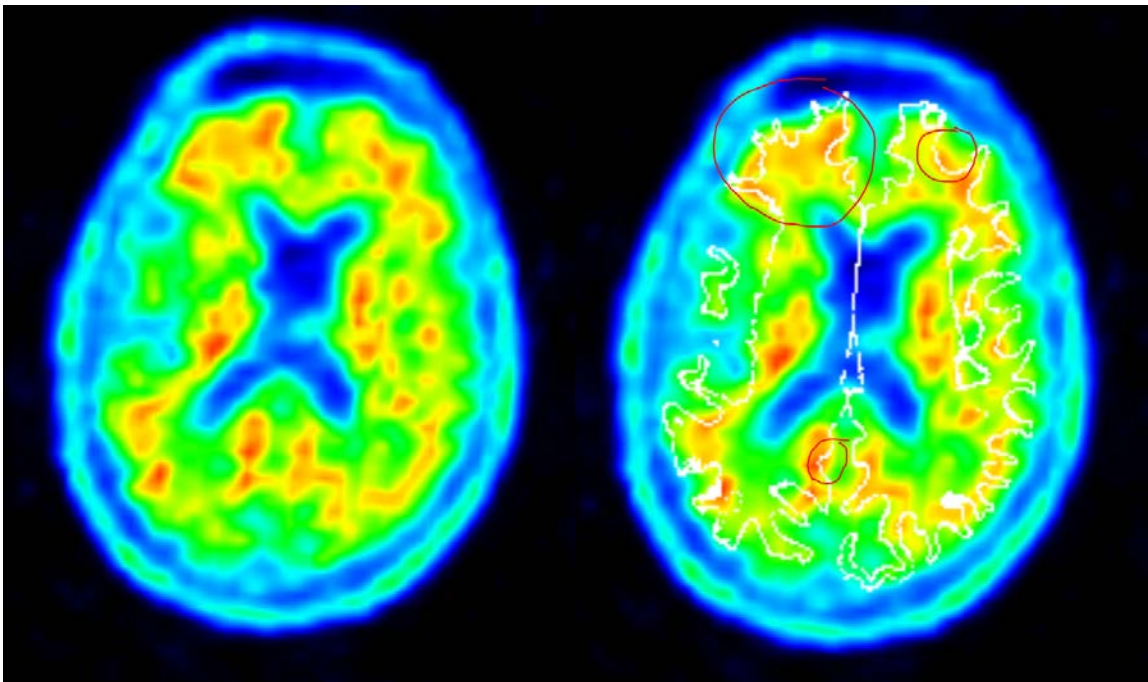


Figure 4-12: Left is the PET Image without White Matter Contour, and Right Image is the Same PET with the White Matter Contour; Red Circles Indicate Areas where the Tracer has Spread to the Cortical Regions.

The white matter contour helps experts and non-experts alike rate more effectively the PET scans. Figure 4-13 shows the full Papaya viewer, with the white matter contour, regional SUVR value, and region name. With this information at hand, it is possible to know that in the rostral middle frontal region the SUVR is 1.49 (higher than the threshold for a Florbetaben and Florbetapir PET scan), and also that the tracer has spread to this area.

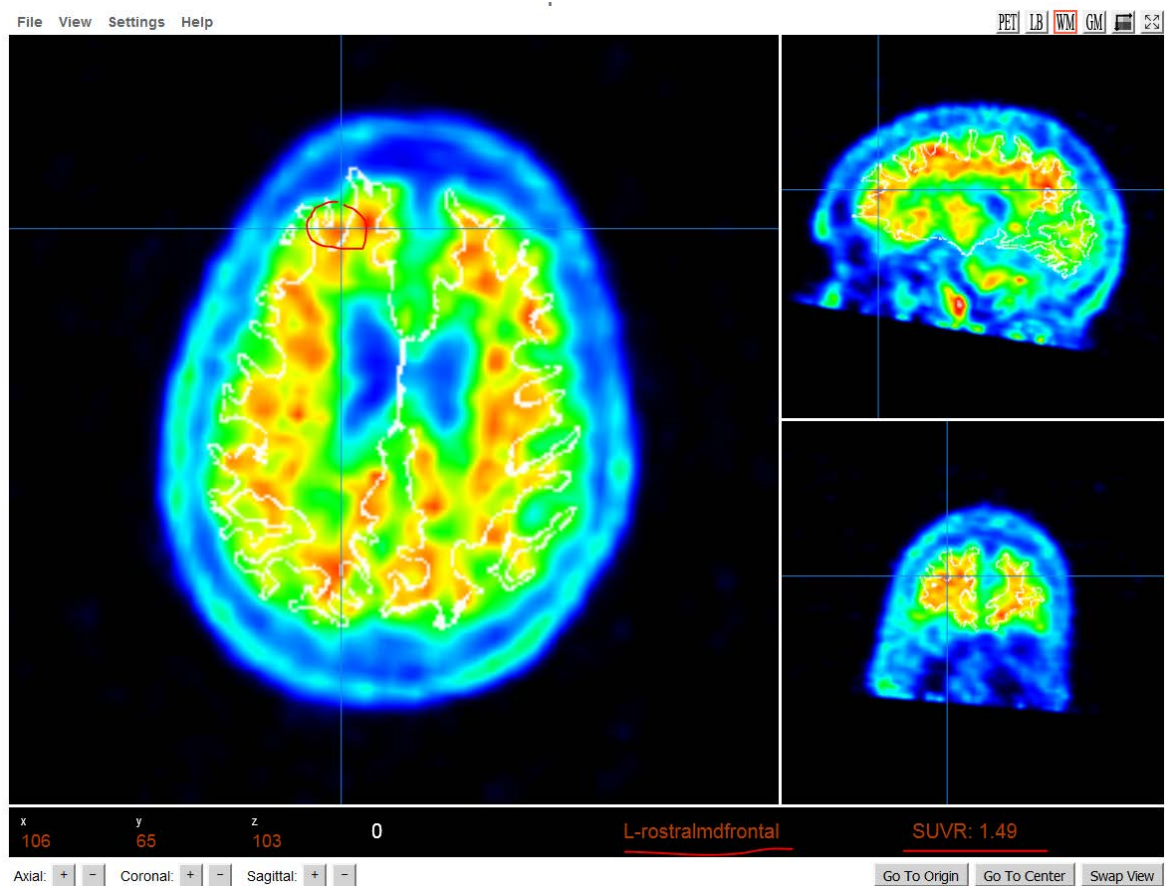


Figure 4-13: Full Papaya Viewer with White Matter Contour, showing SUVR Value, and Anatomical Region Name.

#### 4.10 Heat maps

One of the advantages of NWSI is the visualization component. Heat maps are a powerful way of inspecting data. Essentially, values are assigned to FreeSurfer regions, and a gradient of colors is overlaid on a T1 images representing these values. In a two-colored heat map (i.e.: Blue/Red), lower values will be bluer, while higher values will contain more of the red color. These values represent a specific measure, for example regional atrophy, or SUVR value. They could also group FreeSurfer regions into larger sets (such as frontal, parietal, etc.) and represent each larger region with the same color.

A form was developed to display regional information as heat maps. The form lets the user select an MRI from a list and use the output from an excel document to color the T1 image. The form is built with JavaScript, allowing a responsive and interactive interface. The form is capable of representing any set of measures as a heat map, as long as such measures can be converted into specific regional values. For illustrative purposes, Figure 4-14 represents the cortical and subcortical volumes. The left cortical regions were assigned a value of 1; the right cortical regions a value of 4. The subcortical regions were assigned values 2 (left) and 3 (right), respectively.

Figures 4-15 and 4-16 show visualization examples of the SUVR values in an AD patient and control subject, respectively. Subjects are classified as positive or negative SUVR depending on the amount of amyloid load that has deposited into certain cortical regions. Figure 4-15 has little color contrast between cortical and subcortical regions. This indicates that the depositions of SUVR in cortical regions are similar to the ones observed in the white matter.

It is also noticeable that frontal regions have lower contrast with their surrounding white matter regions, while occipital regions have more contrast. This is consistent with the way amyloid deposits in AD. Figure 4-16 has a higher contrast between cortical and subcortical regions, which is indicative of lower amyloid depositions in the cortical regions.

Figure 4.17 shows another type of heatmap focusing on the cortical volumes, where an expert could visualize which regions have atrophied. Each region represents its own cortical volume. Regions colored with deeper shades of red have larger volumes. For this Figure a Yellow/Red color map was used instead.

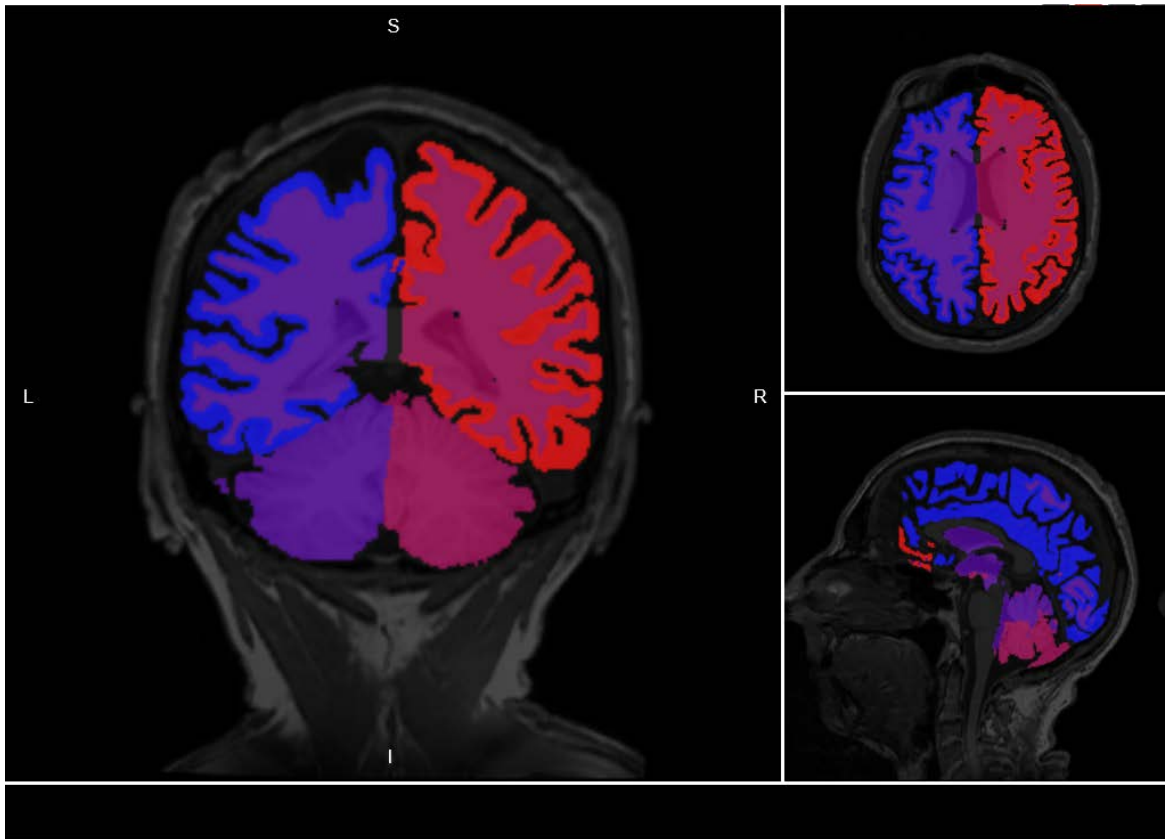


Figure 4-14: Heat map of Cortical and Subcortical of Right and Left Hemisphere.

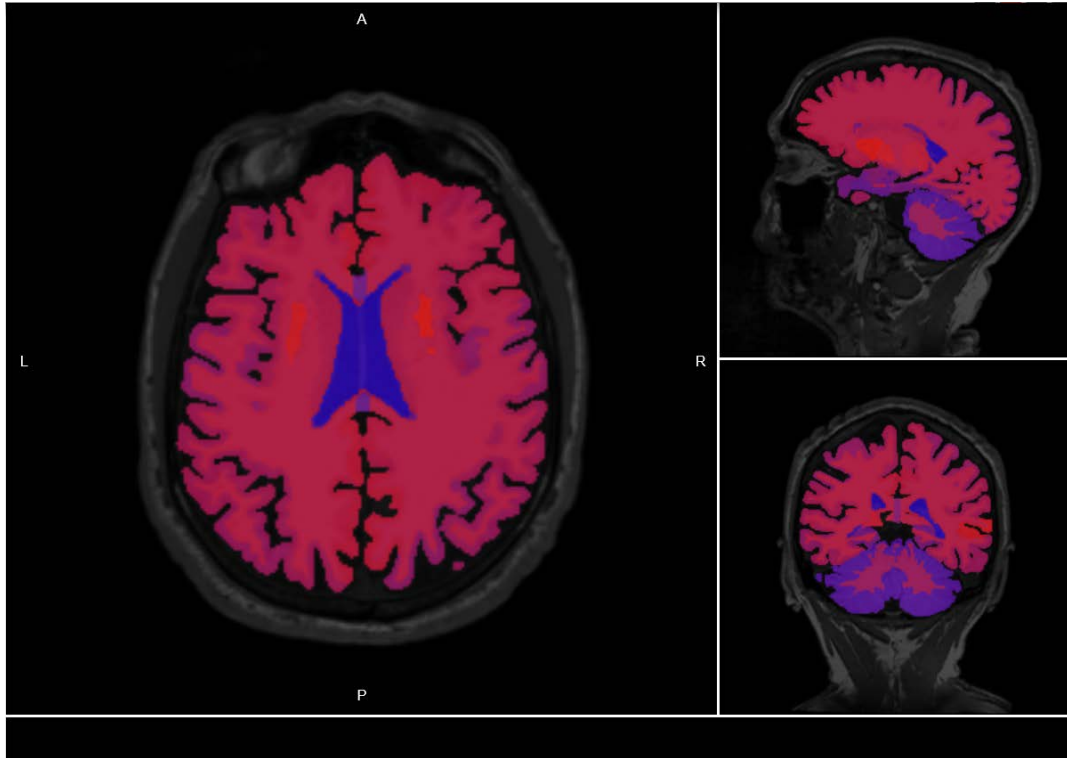


Figure 4-15: Heat Map of AD (Amyloid Positive) Subject.

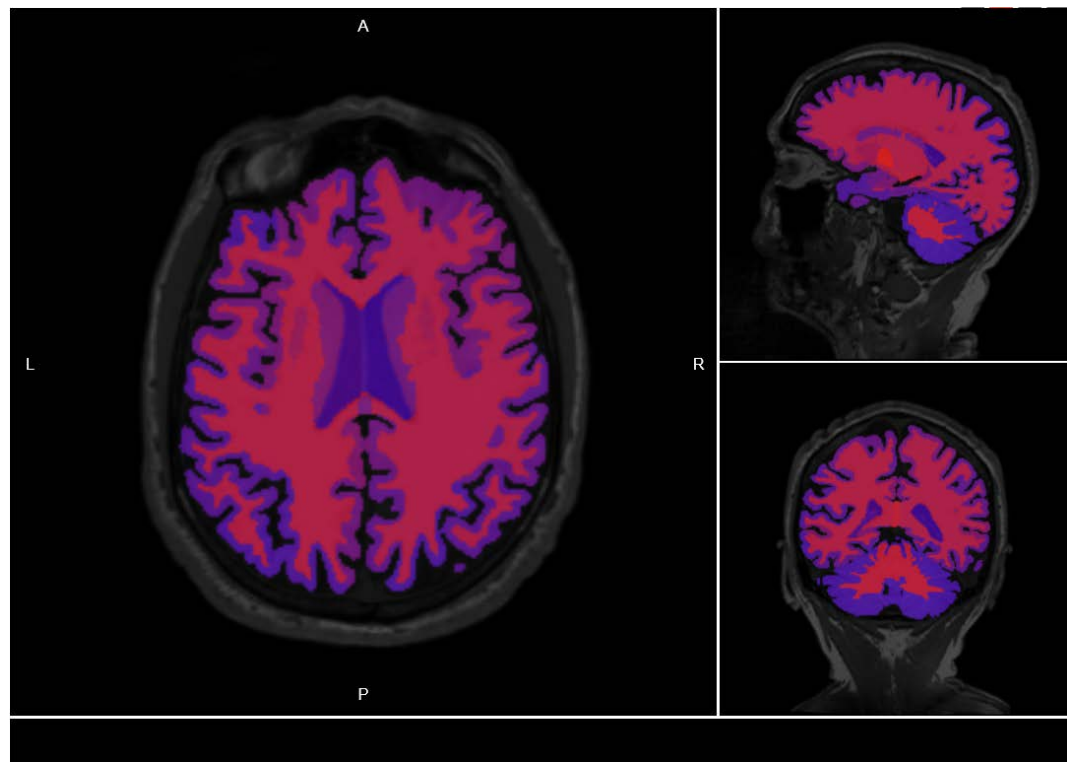


Figure 4-16: Heat Map of Control (Amyloid Negative) Subject.

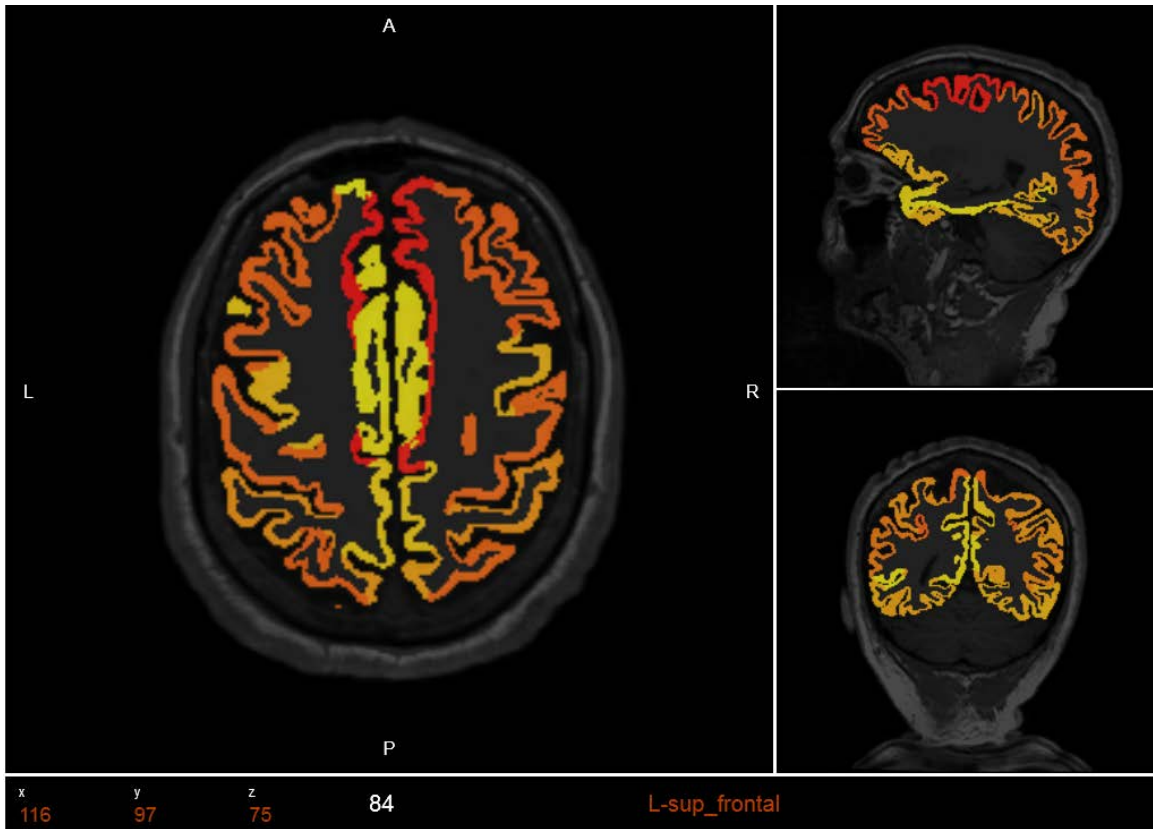


Figure 4-17: Represents the cortical volumes. Each region was assigned the value of its volume. Regions colored with deeper shades of red have larger volumes. For this Figure a Yellow/Red color map was used instead.

Given that the values modeled come from NWSI subjects, the heat maps can be created for the same subject they were calculated for. The heat map form allows modeling the properties on the same brain, even if the values come from different subjects. This provides a common platform for visualization. This makes it possible to model properties from subjects obtained from other sources (not in NWSI). Regions with a value of -1 will not be displayed; that way only selected regions will be visible.

The current implementation does not store heat maps on the server. The users of the interface can store these reusable heat maps in excel at their local computers. Besides the colors, the viewer also displays the region name as the mouse hovers over the region.

In epilepsy, differently than for AD, the goal is to detect the epilepsy focal region in the brain where seizures are thought to emanate from. We have studied the correlation between PET/MRI-Volumes and epileptogenicity maps having been explored with Electroencephalography (EEG). The significance of the results suggests that interictal FDG-PET/MRI-Volumes and ictal EEG activity may share some common underlying pathophysiologic mechanisms of ictogenesis, and by combining all features may help to identify the seizure-onset zone with a higher accuracy. Unbalance in brain regions originated by activity, as measured through PETs, or atrophy, as measured by volumes, can be visualized as heat maps by coloring the regions by SUVR values or regional volumetric measurements.

Figure 4.18 below shows a heat map of volumetric measurements. By comparing the difference in color in regions on the left and right hemispheres, asymmetry can be evaluated. The volume of the superior temporal lobe is smaller to the left when compared to the right. There is an evident asymmetry between these 2 homologous regions. These homologous regions also show asymmetry when SUVR values are compared. These results validate the 3D source location of this patient since the left temporal region is the presumed epileptogenic region, as shown in Figures 14.19 and 14.20.

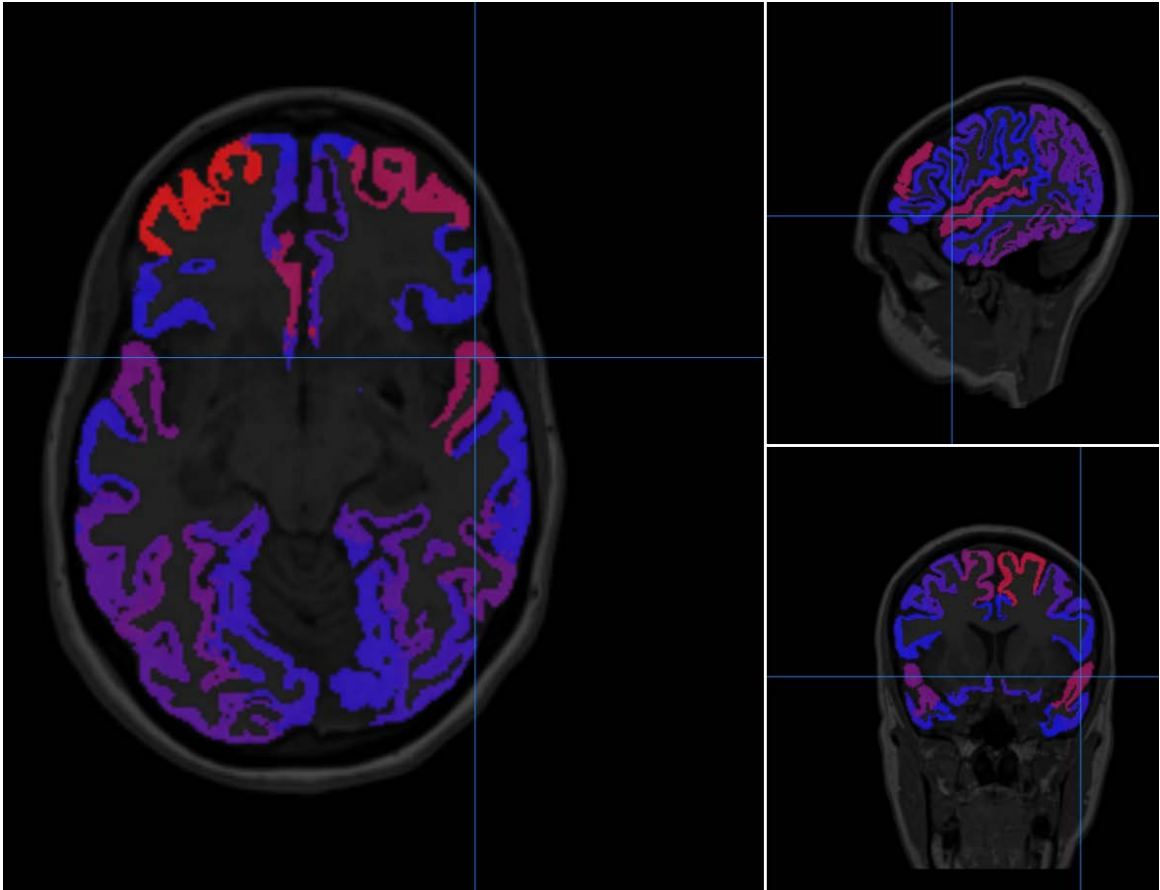


Figure 4-18: Slice of a heat map Epilepsy subject showing asymmetry between homologous regions. The volume of the left temporal lobe is smaller when compared to the right.

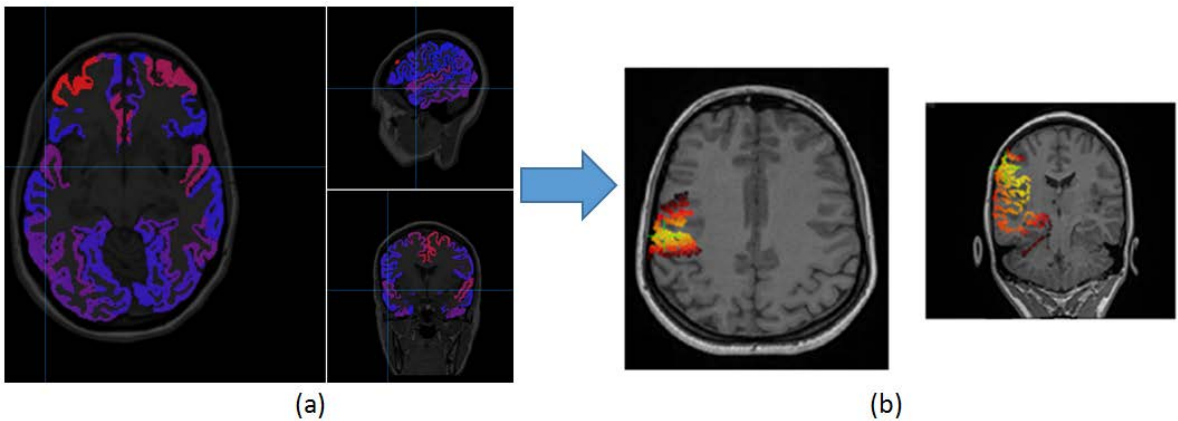


Figure 4-19: The 3D source solution (b) is also indicating the superior temporal region as the source of the seizure; the volume asymmetry (a) is also evident in the same region.

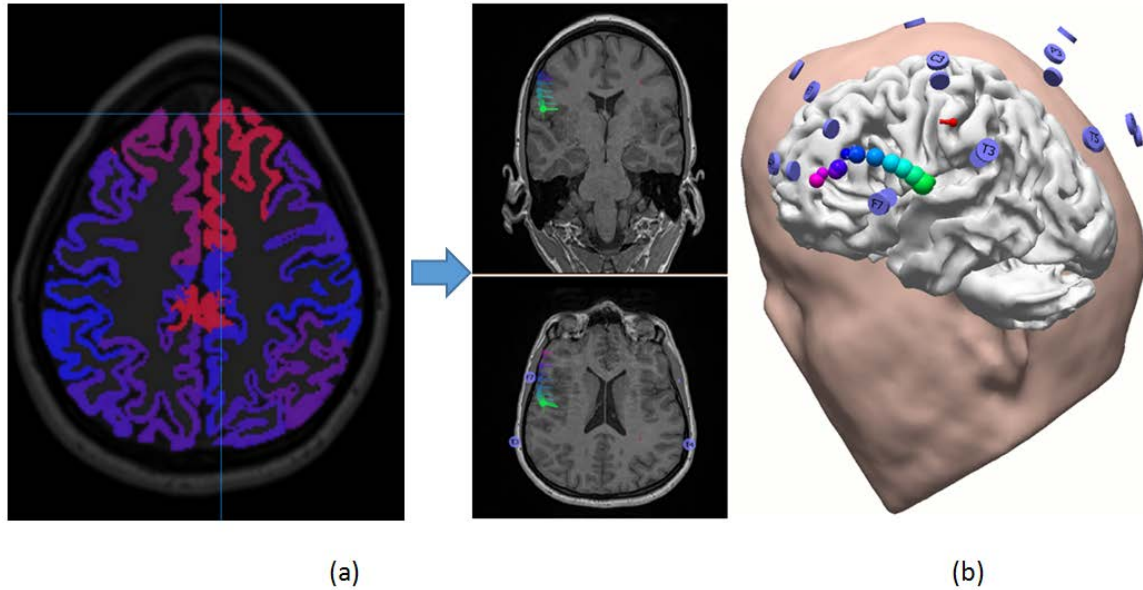


Figure 4-20: Volume of the Superior frontal region (a) also shows asymmetry and it also coincides with some 3D results (b).

## 4.11 Image Restoration

### 4.11.1 Introduction

Structural MRI Images are processed to extract features such as regional volumes, area surfaces and cortical thickness. Algorithms that process these images, such as FreeSurfer (an open source software developed by the Laboratory of Computational Neuroimaging), perform better if the images are acquired free of noise and artifacts [31]. Unfortunately during the acquisition of the images many avoidable or unavoidable errors can occur that translate into artifacts [32]. One common artifact is aliasing: when the FOV (field of view) is smaller than the part of the body scanned, causing a wrap-around of the body part outside the image [33]. The aliasing artifact also causes shading at the edges of the image in the phase-encode direction. Small FOV decreases the duration of scanning. When

scanning the brain many technicians chose the smallest possible FOV to save time. Aliasing artifact can be corrected by increasing the FOV at the time of the scan. If the scan cannot be repeated because of patient follow-up issues, methods must be developed to deal as best as possible with these corrupted images.

Alzheimer's disease does not reflect prominently in the occipital regions [34], but an underestimation due to shading in the occipital area will cause an underestimation of brain size, or intracranial volume (ICV) [35]. ICV is an important metric in inter-patient studies, often used to correct for brain size. As a consequence, this study proposes a new method to restore the image with shading artifacts. The shading of the occipital regions reduces the range of the values, causing pixels with different values to be equal. There is no way to restore the image and separate those equal pixels since the information is lost. N3 and N4 algorithms [36] (nonparametric non-uniform intensity normalization) were tried, but could not correct the strong signal loss. Enhancing contrast methods were tried, but they were found to be time consuming given the number of images to process [37].

Included in this implementation are 207 volume MRI images (out of a total of 223) that displayed occipital shading but were acquired with the Skyra MRI machine. All were acquired as part of the 1Florida ADRC cohort, taken from 2016 to 2018. The proposed image restoration method begins by selecting a random sample of 25% of the images and extracting the brain with the Brain Extraction Tool (BET). The brain extraction is visually inspected to make sure it contains the shaded area. BET can be parametrized to extract more, or less of the brain matter. These extracted brains are quality controlled and processed in FSL FAST (FMRIB's Automated Segmentation Tool). FAST is an

automated algorithm that creates a segmentation of the brain into white and gray matter, outputting also the average pixel values for white and gray matter. Then, starting from the first slide at the edge, the brain is traversed until a slide is found that is within 5% of these averages (each slide is treated as mixture of Gaussians, and the histogram's intensity ranges are scaled). This slide indicates where the shading artifact dissipates. Then, starting on that slide we go back to previous slides recording the averages until we exit the brain. These values are used to create a model describing the shading. Experts in the field of image processing know full well that image restoration is perhaps the most challenging of tasks as we always struggle to define all the parameters of the transfer function or of the degradation process that led to a less than perfect image acquisition process. Hence, as we cannot achieve full restoration, it was deemed sufficient to restore intelligently the pixel intensities enough for FreeSurfer to extract the whole brain and overcome the presence of shading. A java Application was developed that uses the parameters modeled (threshold, start and end slides, white matter, gray matter averages). The intensity in the shaded areas is increased according to the model, and the image is saved and re-processed by FreeSurfer.

Medical images often contain artifacts: Anomalies of the visual representation of the image. These artifacts are features that were not present in the original image and prevent algorithms from correctly interpreting and processing the images. The ADRC data was plagued by wrap-around artifacts that caused shading in the frontal and occipital regions. Some images, where the aliasing overlapped the main central image were discarded, see Figure 4.21. Others can be corrected, since only shading was present, see Figure 4.22.

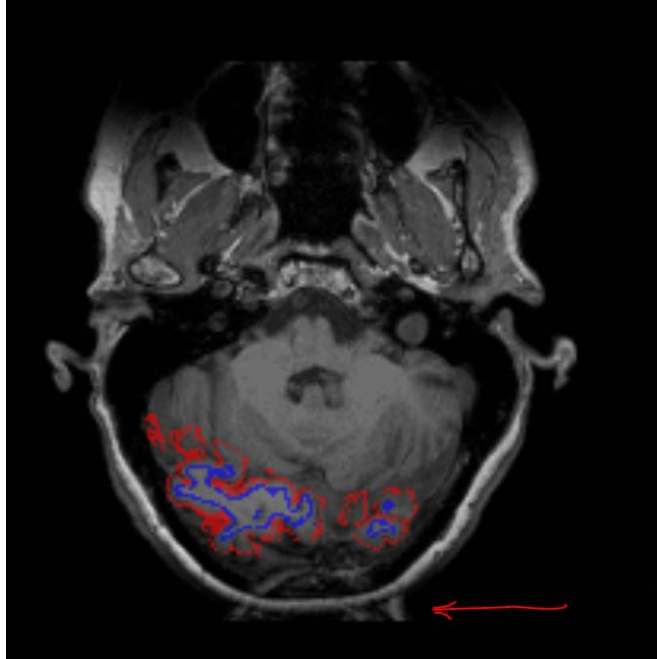


Figure 4-21: Aliasing Artifact Overlapping the Occipital Region. This Image is not Usable as the Two Signals Overlap Resulting in Erroneous Results.

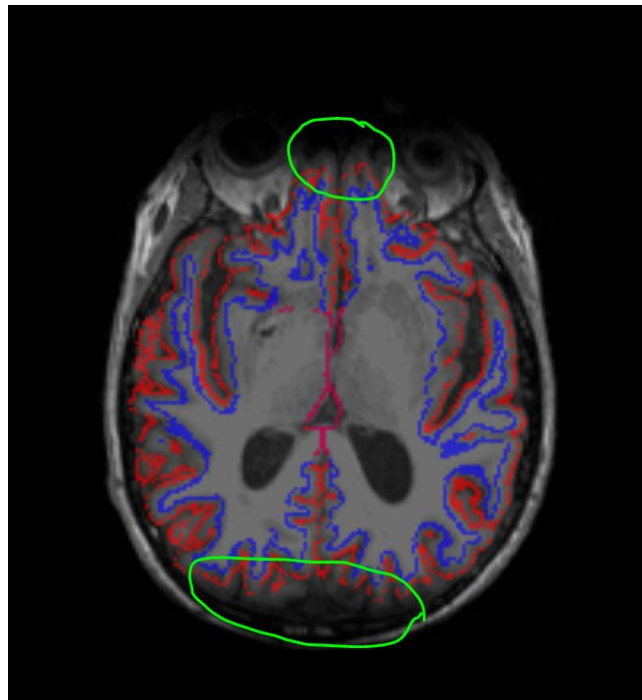


Figure 4-22: Shading in the Occipital and Frontal Regions Prevent FreeSurfer from Segmenting the Image Correctly. The Blue and Red Lines Represent the White and Gray Matter Respectively.

#### **4.11.2 Problems arising from Shading**

During image acquisition, once the signal loss darkens the image, the range of values is altered. Once two pixels acquire the same value in the reduced range, they become indistinguishable and cannot be restored to their original values. Luckily, most of the shading was observed in the occipital area, which is not considered important in regions prone to AD.

Nonetheless, to avoid any risk of faulty measurements, especially in estimating intracranial volume (ICV), a method was created through the NWSI interface to model the loss of signal and restore the images to an approximation of the original images, allowing as a consequence FreeSurfer to register the whole brain and segment the whole volume. Some underestimations will occur in the occipital cortical values that are irrelevant to AD, but FreeSurfer will be able to see the whole brain and estimate the ICV (Intracranial volume) correctly. Also, as the rest of the image remains unchanged FreeSurfer will estimate the same volumetric values for the unaffected regions: such as the Hippocampus and precuneus.

The ICV value is fundamental for experiments using volumetric regional values. Inter-subject brain sizes are adjusted by dividing the regional volumes by the ICV. The ICV value is not expected to change significantly for the same adult subject. Brains that are atrophied will also keep the same ICV because the ICV is measured from the Dura matter (the outermost membrane enveloping the brain).

### 4.11.3 Methodology for Image Restoration

ADRC subjects that contained frontal and occipital shading with no overlapping aliasing were selected and uploaded into the NWSI web interface in order to obtain the FreeSurfer results. Figure 4.23 shows subject 1, where noticeable shading highlighted in green could lead to an underestimation of the brain volume. The ICV reported by FreeSurfer was estimated as 1277405.93 mm<sup>3</sup>.

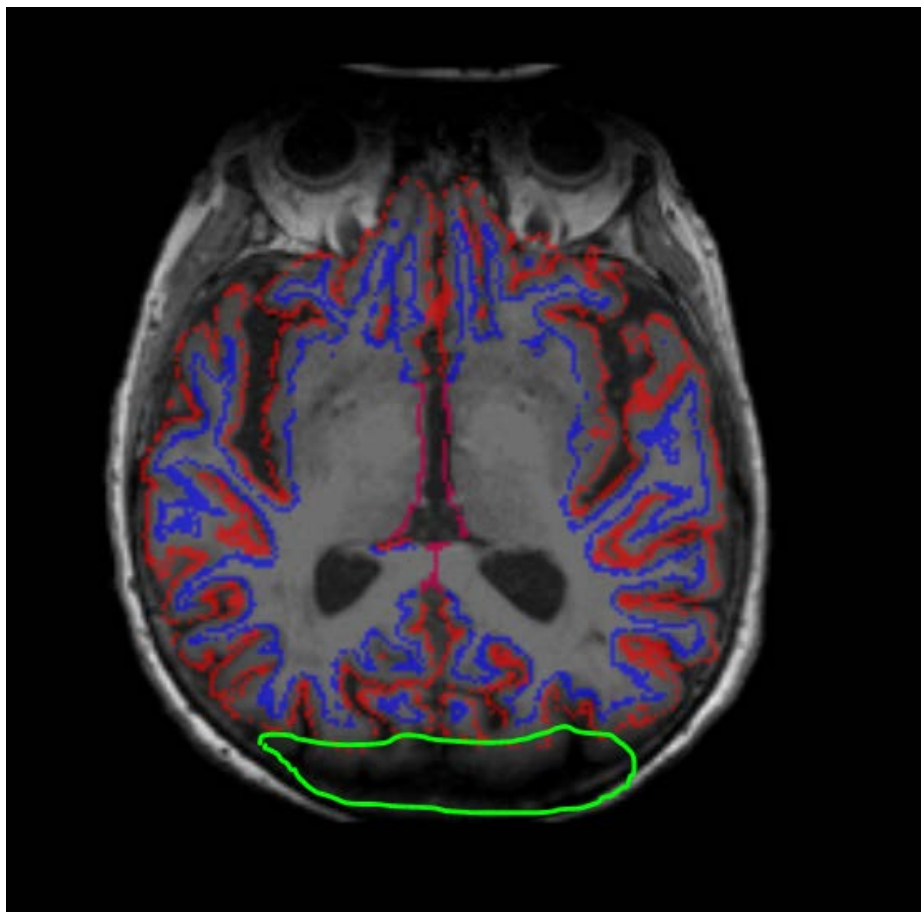


Figure 4-23: Subject 1 Processed by FreeSurfer with Underestimated Brain Size (Shading is Indicated by the region highlighted in Green). The Blue and Red Lines Represent the White and Gray Matter, Respectively.

To overcome such incorrect volume estimations, 25% of the images were randomly selected and an image restoration model was created using the following steps:

- (1) Extract the brain with the BET tool. Once the brain is extracted the skull is removed, and the only intensities present in the image are associated to brain tissue, as illustrated in Figure 4.24.
- (2) Execute FSL FAST to estimate the BIAS field and white/gray matter segmentations and related intensity averages.
- (3) Find, from the last slide (stepping forward), the slide where the average of white and gray matter intensity averages is within 5% of the value reported by FLS FAST as can be observed in Figure 4.25. (This will detect the slide where the shading artifact dissipates).
- (4) Increase the brightness of the shaded slides until the averages are within 5% of the expected intensities reported by FSL FAST. As the shading is gradual slides closer to the edge will be darker.
- (5) Find the minimum threshold that will increase the brightness of the brain, but not the background (if the background values are increased a band will be visible in the areas outside the brain).
- (6) Average these values for all images and save the parameters.
- (7) Perform steps 1-6 for the frontal region.

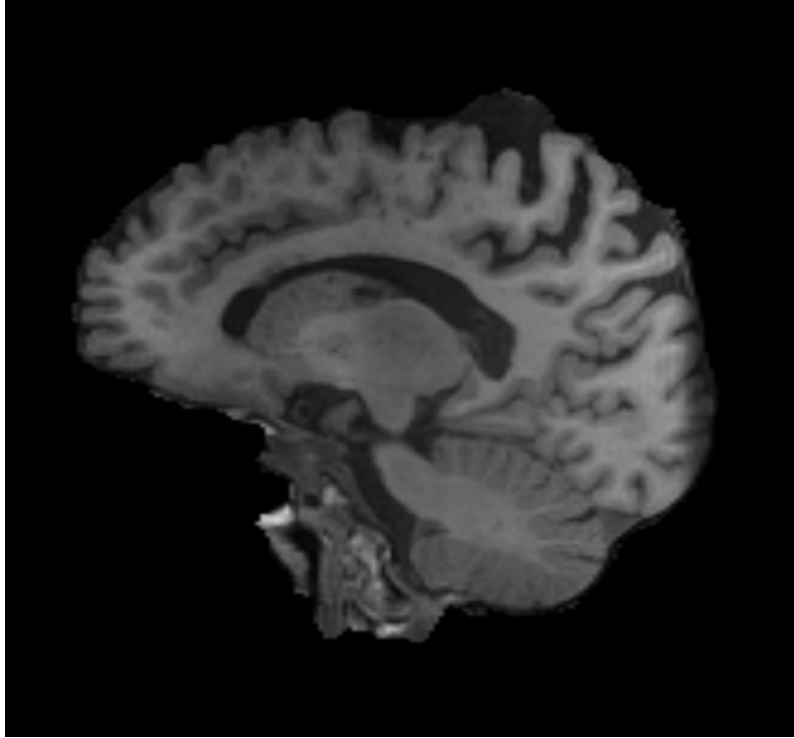


Figure 4-24: Extracted Brain, with visible shading in the occipital region.

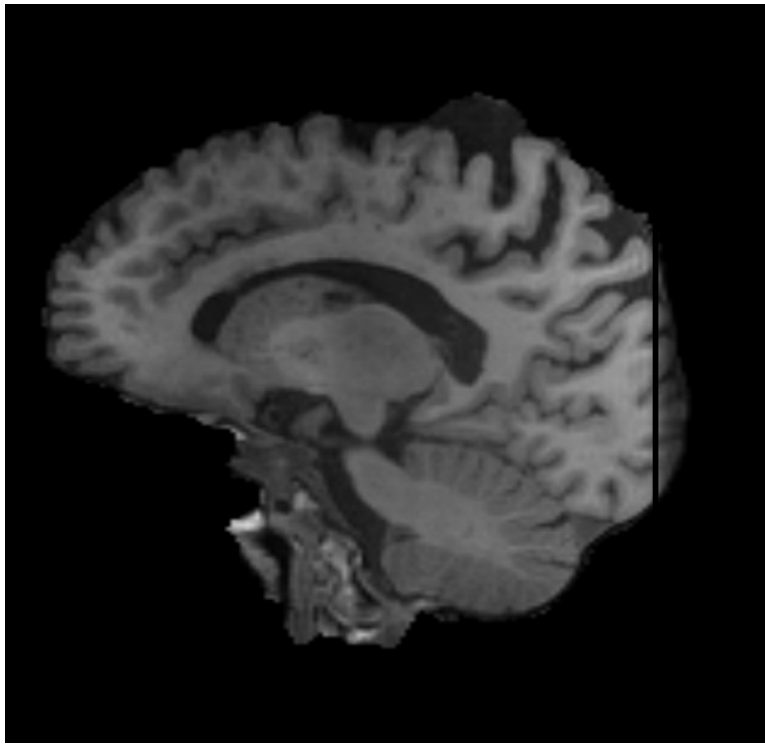


Figure 4-25: Slide where the Average Values of Gray and White Matter are within 5% of the Ones Reported by FSL FAST.

A Java application was developed to open the MRI image files and perform the changes to all the images in a batch job. The new corrected images were uploaded to NWSI. Figure 4.26 contains Subject 1, before and after the correction. Subject 1 was used as a model because two other MRIs were present in the data base with the expected ICV. The other two ICV values were  $1375730.91 \text{ mm}^3$  and  $1387010.24 \text{ mm}^3$ , which are within the expected error for intra-subject ICV values. The reported ICV of the corrected image is  $1367832.66 \text{ mm}^3$ .

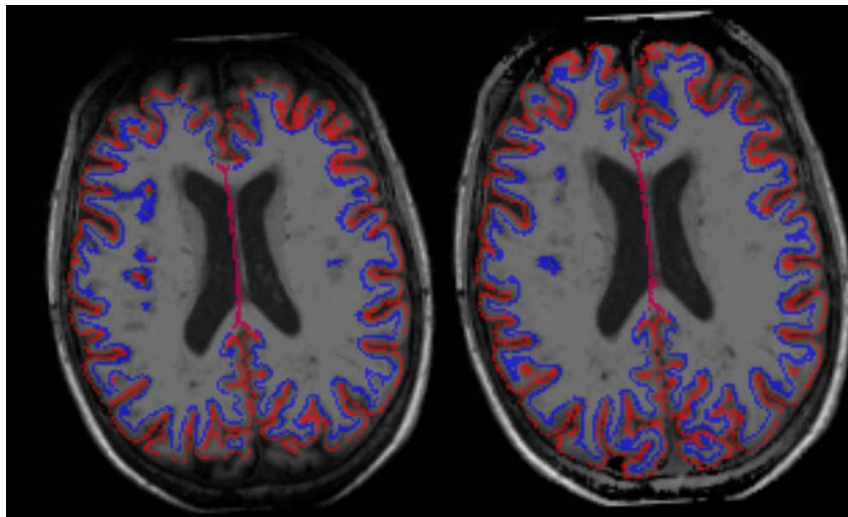


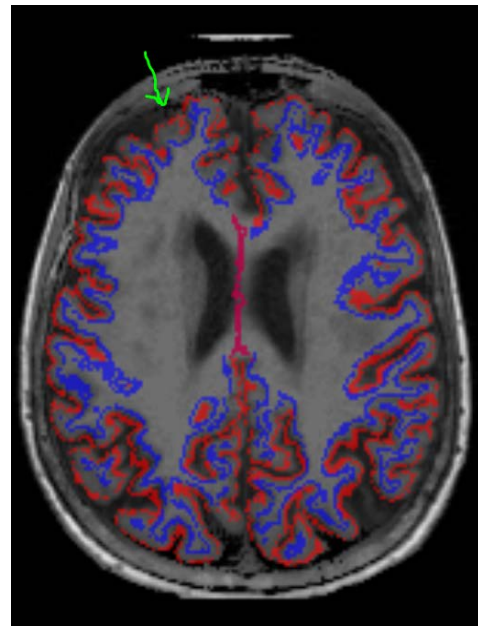
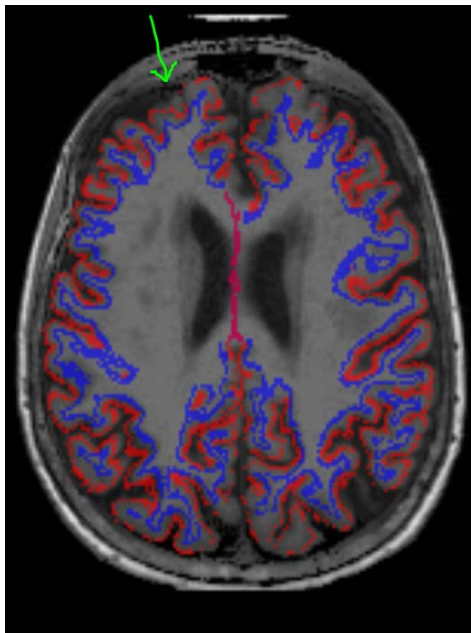
Figure 4-26: Subject 1 on the left with no correction,  $\text{ICV} = 1277405.93 \text{ mm}^3$ . On the right Subject 1 with the corrections,  $\text{ICV} = 1367832.66 \text{ mm}^3$  (diff=6.6%) The red and blue lines cover the whole brain volume. The blue and red lines represent the white and gray matter.

#### 4.11.4 Restoration and Dependence to Type of MRI Scanner

When the restoration model was applied to all MRIs that presented shading, we discovered that the performance of the model was extremely good for all MRIs acquired more recently with the Skyra MRI machine that was newly acquired at the Wien Center for Alzheimer's disease and Memory Disorders at Mount Sinai Medical Center.

Coincidentally, the same restoration model did not perform as well on those older MRIs acquired through a different scanner (26 MRI volumes out of 207). To prove our point, patient 110004 was processed using both restoration models, as can be observed from 4.27. The new ICV using Model 2 is 1369666.25147, while the previous one using Model 1 was 1367832.66104).

The new corrections improve the segmentation in the frontal cortex. Some regions that were missing from the segmentation are now part of it. This might not seem like a significant improvement, but those cortical regions are very thin, and any bit of it that we account for could affect the results. This is especially true in the frontal cortex, as this case has shown, that is deemed so important for AD classification and prediction.



Restoration Model 1-based Correction.

Restoration Model 2-based Correction.

Figure 4-27: Restoration dependency on Scanner Type: with older-MRI-based ICV (Model 1) being ICV: 1367832.66104 and new ICV from the more recent MRIs (Model 2) found to be increased to 1369666.25147 (diff=1.34%) The red and blue lines are the gray and white matter.

We determined that patient 110004 was not an extreme case in comparison to the other 16 scans acquired pre-Skyra, it is just because we noticed those missing cortical sections, which are relevant in AD. But most of the other 16 scans should improve calculations of the ICVs much significantly.

#### **4.11.5 Merits of the Proposed Image Restoration Methodology**

The proposed method partially restores the structural MRIs and allows for more accurate estimations of the ICV measure. All the MRI images were obtained using the same scanner and apparently under the same conditions, so the created model 1 was applicable to all 207 MRI volumes. As we have demonstrated, this method can be modified to create a different model (e.g. Model 2) which was created for the other 16 MRI volumes which acquired using a different MRI machine and which has introduced different form of shading.

FreeSurfer has a method that allows a user to create control points in the white matter in order to increase brightness in the vicinity of the point. But this will mean that each image will have to be opened and edited individually. Processing 207 images will probably take a month or longer. The method proposed is capable of creating a model and process the images in a few minutes, with no human interaction.

#### **4.12 SVM Classification**

While the SVM classifier was designed to be used with any dataset provided by the user, we calibrated it and tested it with our datasets. Each experiment was iterated 50 times, each iteration dividing the data in a new random pattern: Tables 4-1 to 4-4 below show

the results of the experiments with the ADNI dataset for the different binary classifications.

#### 4.12.1 Control vs. AD, RBF Kernel, corrected for ICV

Table 4-1 shows the results from running the interface for Controls vs. AD, selecting linear scaling, RBF kernel, and correcting for ICV.

#### 4.12.2 Control vs. AD, Linear Kernel, corrected for ICV

Table 4-2 shows the results from running the interface for Controls vs. AD, selecting linear scaling, linear kernel, and correcting for ICV.

#### 4.12.3 Control vs. aMCI, Linear Kernel, corrected for ICV

Table 4-3 shows the results from running the interface for Controls vs. aMCI, selecting linear scaling, linear kernel, and correcting for ICV.

Table 4-1: Control vs. AD, with RBF Kernel, Linear Scaling, correcting for ICV.

|     |             |      |
|-----|-------------|------|
| SV* | Sensitivity | 0.82 |
|     | Specificity | 0.91 |
|     | Accuracy    | 0.89 |
| HS* | Sensitivity | 0.71 |
|     | Specificity | 0.89 |
|     | Accuracy    | 0.83 |
| CV* | Sensitivity | 0.68 |
|     | Specificity | 0.92 |
|     | Accuracy    | 0.84 |
| TA* | Sensitivity | 0.71 |
|     | Specificity | 0.95 |
|     | Accuracy    | 0.87 |
| SA* | Sensitivity | 0.45 |
|     | Specificity | 0.84 |
|     | Accuracy    | 0.70 |

\* SV: Subcortical Volumes, HS: Hippocampal Subfields, CV: Cortical volumes, TA: Thickness, SA: Surface Areas

Table 4-2: Control vs. AD, with linear kernel, linear scaling, correcting for ICV.

|     |             |      |
|-----|-------------|------|
| SV* | Sensitivity | 0.81 |
|     | Specificity | 0.91 |
|     | Accuracy    | 0.88 |
| HS* | Sensitivity | 0.76 |
|     | Specificity | 0.89 |
|     | Accuracy    | 0.84 |
| CV* | Sensitivity | 0.69 |
|     | Specificity | 0.88 |
|     | Accuracy    | 0.82 |
| TA* | Sensitivity | 0.73 |
|     | Specificity | 0.93 |
|     | Accuracy    | 0.86 |
| SA* | Sensitivity | 0.55 |
|     | Specificity | 0.81 |
|     | Accuracy    | 0.72 |

\* SV: Subcortical Volumes, HS: Hippocampal Subfields, CV: Cortical volumes, TA: Thickness, SA: Surface Areas

Table 4-3: Control vs. aMCI, with Linear Kernel, Linear Scaling, correcting for ICV.

|     |             |      |
|-----|-------------|------|
| SV* | Sensitivity | 0.65 |
|     | Specificity | 0.80 |
|     | Accuracy    | 0.73 |
| HS* | Sensitivity | 0.66 |
|     | Specificity | 0.80 |
|     | Accuracy    | 0.74 |
| CV* | Sensitivity | 0.61 |
|     | Specificity | 0.75 |
|     | Accuracy    | 0.69 |
| TA* | Sensitivity | 0.53 |
|     | Specificity | 0.74 |
|     | Accuracy    | 0.65 |
| SA* | Sensitivity | 0.50 |
|     | Specificity | 0.67 |
|     | Accuracy    | 0.59 |

\* SV: Subcortical Volumes, HS: Hippocampal Subfields, CV: Cortical volumes, TA: Thickness, SA: Surface Areas

#### 4.12.4 Control vs. AD, Linear Kernel, corrected for ICV, and using MMSE

Table 4-4 shows the results from running the interface for Controls vs. AD, selecting linear scaling, linear kernel, correcting for ICV, and using the MMSE score in the classification.

Table 4-4: Control vs. AD, with Linear Kernel, Linear Scaling, correcting for ICV, using MMSE. \* SV: Subcortical Volumes, HS: Hippocampal Subfields, CV: Cortical volumes, TA: Thickness, SA: Surface Areas.

|     |             |      |
|-----|-------------|------|
| SV* | Sensitivity | 0.91 |
|     | Specificity | 0.95 |
|     | Accuracy    | 0.94 |
| HS* | Sensitivity | 0.83 |
|     | Specificity | 0.92 |
|     | Accuracy    | 0.89 |
| CV* | Sensitivity | 0.83 |
|     | Specificity | 0.94 |
|     | Accuracy    | 0.90 |
| TA* | Sensitivity | 0.84 |
|     | Specificity | 0.98 |
|     | Accuracy    | 0.93 |
| SA* | Sensitivity | 0.82 |
|     | Specificity | 0.93 |
|     | Accuracy    | 0.89 |

\* SV: Subcortical Volumes, HS: Hippocampal Subfields, CV: Cortical volumes, TA: Thickness, SA: Surface Areas

When classifying Control versus AD using the RBF kernel and correcting the data for ICV, and in reference to Table 1, results show that accuracy and sensitivity are higher for subcortical volumes and hippocampal subfields. These are expected as Alzheimer's disease is known to affect memory cognition centers that are located among the subcortical regions, where the hippocampus is located. For cortical volumes, thickness areas and surface areas, the results are less meaningful.

When using the linear Kernel, as in Table 4.2, results indicate that the linear kernel performs slightly better than the RBF kernel. Table 4-3 shows the classification of aMCI vs. control. Subject with aMCI are considered to be potentially closer to developing AD, and certain volumetric difference can be classified. However, the accuracy is much lower than on the previous experiments; this is because aMCI patients don't have the advanced level of brain atrophy that AD patients have.

Finally, table 4-4 shows the effect of including the MMSE score in the classification. Across all measurements, the sensitivity, specificity, and accuracy improved to almost 90%. As reported by the literature, experts rely heavily on neuropsychological scores to diagnose AD and MCI stages. This creates a dependency, or bias, in the data with respect to the MMSE score. Many experts recommend to not use the MMSE score in supervised learning algorithms given that the class separation will already come biased by the MMSE score. The machine learning realm contains other algorithms that don't have this problem. The unsupervised learning family of algorithms, such as clustering, allows finding clusters of data that are similar to each other.

The effect of the MMSE score in the classification also exemplifies why feature selection does not play a key role on this implementation of SVM. The algorithm is already optimized to find the more significant features.

The Data balancing effect is not studied in our experiments. The ADNI data has a much larger number of controls when compared to the AD subjects. The consequence is a higher specificity value. In the ADNI data there are almost double the number of controls than AD subjects. This means that the training size is larger for controls, as well as the

classifiable control sample. The algorithm is better trained to detect controls, thus reporting a higher specificity. A review of the literature shows that our classifier is as good as those reported by other authors, as shown in table 6-1.

Table 4-5: Performance average comparison of AD/Control Classification.

| AUTHORS             | DATASET(AD/CN)   | Sensitivity | Specificity | Accuracy |
|---------------------|------------------|-------------|-------------|----------|
| Zhang (2011) [38]   | ADNI(51/52)      | 86%         | 86%         | 86%      |
| Magnin (2009) [39]  | Private(16/22)   | 91%         | 96%         | 94%      |
| Kloppel(2008) [40]  | Private(33/57)   | 60%         | 93%         | 81%      |
| Walhovd (2010) [41] | ADNI(42/38)      | 81%         | 83.50%      | 82%      |
| Cuingnet(2011) [42] | ADNI(162/137)    | 81%         | 95%         | -        |
| Zhou (2014) [43]    | Private{ 127/59) | 84%         | 96%         | 92%      |
| Proposed Classifier | ADNI(139/76)     | 82%         | 91%         | 89%      |

## 5 Validation Tests

### 5.11 MRI Values Validation

As cautioned earlier, FreeSurfer values obtained from the same FreeSurfer version can vary among different hardware and software platforms. According to the FreeSurfer team, this is due to OS-dependent libraries that support FreeSurfer. Hence, for this proposed web interface, the replica servers (RSs) are calibrated, making sure they always provide the same results before they are deployed. ADNI renders FreeSurfer results calculated on FreeSurfer 5.1.

In order to validate NWSI, a paired T-test was performed to compare the values reported in the ADNIMerge file and the NWSI results. 20 ADNI cases were selected at random from the 4 main diagnoses ([AD, Early Mild Cognitive Impairment (EMCI), Late Mild Cognitive Impairment (LMCI), and Cognitively Normal (CN)]). One of the selected subjects failed ADNI's quality control for the MidTemporal region, but it was successfully processed by NWSI. See Table 1 below for the obtained results.

ADNIMerge and NWSI FreeSurfer results are highly correlated. There is a small statistical difference for MidTemporal and Entorhinal cortex. ADNIMerge was processed with FS5.1, and NWSI uses FS5.3. FreeSurfer 5.3 was a major upgrade to 5.1. Different FreeSurfer versions produce different results, but it does not imply lack of validity. Classification results can still be reliably used [44]. See Table 5-1 for results.

Table 5-1: MRI Processing by Neuroimaging Web Services Interface (NWSI) Quality Control Comparisons.

| <b>Measure (mm<sup>3</sup>)</b> | NWSI FS 5.3    | ADNI Merge FS 5.1 | Difference (%) | Correlation         | Paired T-Test *   |
|---------------------------------|----------------|-------------------|----------------|---------------------|-------------------|
| Hippocampus                     | 7041±1529      | 7043±1404         | -3.00%         | 0.9866<br>(p<.0001) | -0.03<br>(.9788)  |
| Entorhinal Cortex               | 3252±717       | 3504±827          | -6.50%         | 0.876<br>(p<.0001)  | -2.8<br>(.01)     |
| Middle Temporal                 | 19040          | 20020             | -3.40%         | .971<br>(p<.0001)   | -5.3<br>(p,.0001) |
| ICV                             | 1486538±154661 | 1482872±152534    | 2.40%          | 0.9944<br>(p<.0001) | -1.0<br>(0.33)    |

\* H0: Difference=0

### 5.12 18F-Florbetapir PET Validation

NWSI PET SUVR values have been validated with the values on ADNI data as reported by Jagust [45]. All ADNI PET results use 18F-Florbetapir. A random selection of 20 subjects from ADNI was used. Native PETs and MRIs were processed in NWSI, and the calculated global SUVRs were compared to those reported by ADNI. A 2-tailed t-test shows no statistical significance ( $t\text{-Stat} < t\text{ Critical two tails}$ ) as shown in Table 5-2.

### 5.13 18F-Florbetaben PET Validation

NWSI PET SUVR values have been validated using data from the Centiloid Project (CL), as described in the data section above. The 35 subjects were uploaded to NWSI and the results were compared to the ones reported by Dr. Rowe. A 2-tailed t-test was done on the processed data and no statistical significant difference was found, see table 5-3 comparing the NWSI values to the ones reported by the CL team.

These results are important because the CL team performed the registration and calculation using SPM8. It validates NWSI not only with other versions of FreeSurfer, but also with other software packages that provide segmentation and parcellation.

Table 5-2: T-Test-Paired comparing NWSI and ADNIMerge 18F-Florbetapir PET Global SUVR values.

|                              | NWSI  | ADNIMERGE |
|------------------------------|-------|-----------|
| Mean                         | 1.22  | 1.217     |
| Variance                     | 0.047 | 0.044     |
| Observations                 | 18    | 18        |
| Pearson Correlation          | 0.93  |           |
| Hypothesized Mean Difference | 0     |           |
| df                           | 17    |           |
| t Stat                       | 0.26  |           |
| P(T<=t) one-tail             | 0.40  |           |
| t Critical one-tail          | 1.74  |           |
| P(T<=t) two-tail             | 0.79  |           |
| t Critical two-tail          | 2.11  |           |

Table 5-3: T-Test-Paired comparing NWSI and CL 18F-Florbetaben PET Global SUVR values.

|                     | NWSI  | CL    |
|---------------------|-------|-------|
| Mean                | 1.31  | 1.26  |
| Variance            | 0.132 | 0.127 |
| Observations        | 35    | 35    |
| Pearson             | 0.84  |       |
| Hypothesized        | 0     |       |
| df                  | 34    |       |
| t Stat              | 1.25  |       |
| P(T<=t) one-tail    | 0.11  |       |
| t Critical one-tail | 1.69  |       |
| P(T<=t) two-tail    | 0.22  |       |
| t Critical two-tail | 2.03  |       |

## **6 Conclusion and Future Work**

### **6.11 Retrospective**

The initial intent of NWSI is fulfilled in order to create a tool for clinicians and researchers with keen interest on Neuroimaging but do not necessarily have the time and/or the required expertise in image processing, computing, and data management resources. Most of the user interaction with the interface is limited to uploading the data file, requesting the execution of a given task on the uploaded file, and performing quality control on the provided output. The user can select to be notified via email or text message after a long running task has completed.

NWSI initial code was written in 2012. Many details have changed since the original prototype. The feedback provided by medical doctors and other researchers has been invaluable. The system as currently developed is the result of many hours dedicated to understanding the challenges of neuroimaging in brain research and for meeting the needs and requirements of Medical Doctors (MDs). The medical images displayed in the Papaya viewer contain layers defining the edge of the gray and white matter, custom LUTs created based on how MDs visualize the specific results, and many other enhancements which emerged from interacting with the medical team.

### **6.12 Main Findings**

Data entry into NWSI is deemed most effective and user-friendly and has been evaluated based on user feedback. The forms embedded into the interface are intuitive and similar

to many other forms in the Internet. Uploading an MRI into NWSI is as simple as updating a Facebook or Instagram status. Five papers in highly-ranked journals have already been published based on data from NWSI, and several conference papers have been written and published by our graduate students through the use of the NWSI interface.

NWSI is shown to be an effective web platform for storing and processing neuroimaging data. All data is de-identified prior to being uploaded to the server. NWSI is accessible worldwide. The user interacts with the processing pipelines through a simple interactive web-interface, which allows the users to upload and process images of the brain and view the results directly on the browser. The multi-user interface allows for privacy among researchers, as well as data sharing. Data is protected on the secured server, while communication with the user is encrypted. Pipelines which process structural MRI and Amyloid PET scans have been validated with existing and well-established databases. NWSI stores all results in SQL tables and files, facilitating the selection and processing of existing data into new pipelines. As such, NWSI offers a complete solution for Neuroimaging Studies with multi-user tools for data processing and visualization, as well as for downloading to another platform for further processing.

The SVM classifier on the web interface is comparable to other classifiers reported by the literature and allows for the processing of other AD datasets. The results obtained from it are also congruent with the consensus for the effect on volumetric atrophy of Alzheimer's disease. The classifier, as described, will make a great addition to any AD processing pipeline.

Heat maps provide an excellent visualization tool for brain images. Structural MRI images with high resolution can be analyzed voxel by voxel, but PET, fMRI, and DTI images are low resolution and typically a single voxel value is not as important as the average for regions; that is why processing pipelines for these low-resolution modalities study the behavior of regional average. Heat maps provide a simplification of these images by showing the image as processing pipelines study them. They can aid in PET visual rating and validating 3D source localization in Epilepsy.

Visual ratings and binary assessments are the gold standard in AD imaging research. These methods are prone to error and biases when compared to the automated ones, such as the ones implemented in NWSI. Nonetheless, collecting visual ratings allows evaluating the reliability of raters, and can also be used to measure what role rater's expertise plays in the rating process. The NWSI Training website was created on data previously analyzed in NWSI. This new interface connects to the NWSI results and allows for visual rating of PETs and MRIs. Another important question is to measure how expertise and knowledge of the brain anatomy influences the visual rating. Visual ratings are done in the field by inspecting the images and using anatomy knowhow and a rough training to label a PET as positive or negative. But NWSI training displays and labels the regions, removing a layer of complexity from the rating process. NWSI training can provide insights into how non-experts on the field are also able to visually rate PET images correctly just like experts would. Furthermore, the visual rating interface allows a rater located in a different location to collaborate and use a common interface.

Without such an interface it will not be possible to collect this type of data under the control required for this type of study.

Another contribution of this research endeavor is in creating new heat maps which can be a great aid for the visual rating of PET images. Such heat maps are shown to improve the reliability of raters. Heat maps can model regions of the brain by coloring them based on pre-calculated values. When analyzing brain images of low resolution, such as PETs and DTI, the value of a specific voxel is typically not important. The processing algorithms for these images typically produce regional values. By mapping these values into an anatomical T1 image, a visual simplification of the low-resolution image is produced to better represent the processed data.

The NWSI platform allows for users to execute online newly developed machine learning algorithms that were proven to be highly effective in terms of their classification and predictive outcomes. Currently, the interface provides access to an SVM (Support Vector Machine) algorithm to separate binary classes in AD. The algorithm is connected to a sample of the ADNI database. Many of the options are exported to the classification form and can be configured using the interface.

In terms of image restoration, The NWSI interface proposes a method that partially restores the structural MRIs that experience shading in certain regions of the brain. This type of shading that occurs due to some human error in the image acquisition process is found to affect, in a critical way, calculations of the ICV measure and corrupts as well as the volumetric and surface measures of these shaded areas of the brain due to inaccurate image segmentation of the different brain regions. These shading changes, although

found in only small sections of the brain could potentially skew the classification process of the different prodromal stages of Alzheimer's disease. We have shown through this type of image restoration, the ICV values are accurately measured. All the MRI images were obtained using the same scanner and apparently under the same conditions, so the created model was applicable to all. The method can be modified to create a model for each image (or group of images) if they have different rates of shading. In so doing, we have saved time and money for having many of the individuals who have taken these MRIs not to retake them.

We have also proven that the image restoration method that was implemented was also computationally effective. FreeSurfer has a method that allows a user to create control points in the white matter in order to increase brightness in the vicinity of the point. But this will mean that each image will have to be opened and edited individually. Processing 207 images will probably take a month or longer. The method proposed is capable of creating a model and process the images in a few minutes and without need for human interaction.

In terms of image segmentation, another contribution associated with the design of the NWSI interface is in creating a contour as a form of segmentation delineating white matter from gray matter as means to augment the prospects of PET visual ratings. Currently, the gold standard for visually rating PETs is to display them in grayscale and visually assessing the cortical regions in contrast to white matter solely on the basis of brightness level. With the segmentation proposed in this dissertation, the expert rater is able to delineate gray matter from white matter and hence the visual assessment is made

better in terms of gauging the spread of the PET imaging tracer within the white matter area.

On the Centiloid scale, although we have not designed the formula for the conversion to the centiloid scale, we thought that it was important to include such conversion to the centiloid scale into the NWSI platform on the basis of a data collection problem we have personally faced in the design of this web interface. In the process of collecting data for the 1Florida ADRC, we have switched from one company (Amyvid) that provided PET images using the Florbetapir agent to another company (Neuraceq) that provided us PET imaging using the Florbetaben agent. Although both tracers are approved and work equally well, we faced the problem of consolidating these Florbetapir and Florbetaben PET data on a similar scale, the centiloid scale, so that both datasets could be integrated in our processing and statistical analysis.

Through this process, we were able to integrate 185 florbetaben PET images obtained through Neuraceq with the 45 Florbetapir PET images that were acquired through Amyvid. This was quite an exploit as we are capable to maintain all of our patients and normal controls and be able to use all of them in the development of the web interface and related image processing algorithms, and in the statistical analyses that were conducted. This could also accommodate other researchers who may run into similar problem who maybe using one form of these agents and be able to combine their data to other datasets that may have been acquired through a different agent. It is also conceivable that newer PET agents could be developed in the future and that variations of

this scaling method could be implemented to sustain such an integration of PET data acquired under different PET imaging agents.

### **6.13 Future Work**

New studies are added every month to NWSI. As more data is uploaded, it is possible to create methods for merging similar data from different sources. This allows, for example, using the control scans from one account to enhance another study lacking controls. Multimodal pipelines can also be created based on merging PET, structural and functional MRI and DTI. The current implementation does not process fMRI, and the DTI processing is currently very limited. Expanding those pipelines will allow multimodal pipelines to be created for enhanced multimodal studies. New processing pipelines can be exposed to the user, allowing inclusion of previously processed cases and broadening the scope of new studies.

FreeSurfer and FSL were the natural choice for segmentation and registration because ADNI data was available and already processed by FS and FSL. There are other software packages which also provide excellent results: 3D Slicer, AFNI, SPM, etc. As a future development it will be possible to add pipelines employing these software packages and for the user to select which one to use at the upload form.

The heat maps interface allows the visual modeling of regional values. In the examples presented we mentioned that when modeling SUVR values, it can differentiate positive from negative PET scans. The ability to model averages brings raters a step closer to

agreement as one of the mental processes they have to do is precisely estimate this average. Heat maps have the potential to become a tool for aiding raters to reach higher agreements in their results.

The SVM classifier can be used to run additional experiments than the ones reported in this study. More Kernels are available to SVM. The data balancing option might aid in lowering the specificity, but its effect on sensitivity is to be determined. Another great addition will be to study how an unsupervised learning algorithm performs with the MMSE score added. There are other features that can be included in the classification. Genetic traits, SUVR values, resting state fMRI results, and DTI results can be added as features together the volumetric measurements to improve the classification.

The research community needs to put more focus on multiclass classification algorithms to overcome the limitations of binary classifications. More focus should also be placed for multimodal imaging with more advanced machine learning algorithms for both classification and prediction involving longitudinal studies to overcome the collinearity issue of cross-sectional studies.

## LIST OF REFERENCES

- [1] T. Morita, M. Asada, and E. Naito, "Contribution of Neuroimaging Studies to Understanding Development of Human Cognitive Brain Functions," *Front Hum Neurosci*, vol. 10, p. 464, 2016.
- [2] H. Akil, M. E. Martone, and D. C. Van Essen, "Challenges and opportunities in mining neuroscience data," *Science*, vol. 331, pp. 708-12, Feb 11 2011.
- [3] B. Governing Council of the Organization for Human, "Neuroimaging databases," *Science*, vol. 292, pp. 1673-6, Jun 01 2001.
- [4] T. Tuszynski, M. Rullmann, J. Luthardt, D. Butzke, S. Tiepolt, H. J. Gertz, *et al.*, "Evaluation of software tools for automated identification of neuroanatomical structures in quantitative beta-amyloid PET imaging to diagnose Alzheimer's disease," *Eur J Nucl Med Mol Imaging*, vol. 43, pp. 1077-87, Jun 2016.
- [5] H. Kargupta, *Data mining : next generation challenges and future directions*. Menlo Park, Calif. ; LondonCambridge, Mass.: AAAI ;MIT Press, 2004.
- [6] M. W. Weiner, D. P. Veitch, P. S. Aisen, L. A. Beckett, N. J. Cairns, J. Cedarbaum, *et al.*, "2014 Update of the Alzheimer's Disease Neuroimaging Initiative: A review of papers published since its inception," *Alzheimers Dement*, vol. 11, pp. e1-120, Jun 2015.
- [7] L. N. Marengo, R. Wang, A. E. Bandrowski, J. S. Grethe, G. M. Shepherd, and P. L. Miller, "Extending the NIF DISCO framework to automate complex workflow: coordinating the harvest and integration of data from diverse neuroscience information resources," *Front Neuroinform*, vol. 8, p. 58, 2014.
- [8] I. B. Malone, D. Cash, G. R. Ridgway, D. G. MacManus, S. Ourselin, N. C. Fox, *et al.*, "MIRIAD--Public release of a multiple time point Alzheimer's MR imaging dataset," *Neuroimage*, vol. 70, pp. 33-6, Apr 15 2013.
- [9] R. A. Poldrack and K. J. Gorgolewski, "OpenfMRI: Open sharing of task fMRI data," *Neuroimage*, vol. 144, pp. 259-261, Jan 2017.
- [10] K. J. Gorgolewski, G. Varoquaux, G. Rivera, Y. Schwarz, S. S. Ghosh, C. Maumet, *et al.*, "NeuroVault.org: a web-based repository for collecting and sharing unthresholded statistical maps of the human brain," *Front Neuroinform*, vol. 9, p. 8, 2015.
- [11] M. Schirner, S. Rothmeier, V. K. Jirsa, A. R. McIntosh, and P. Ritter, "An automated pipeline for constructing personalized virtual brains from multimodal neuroimaging data," *Neuroimage*, vol. 117, pp. 343-57, Aug 15 2015.
- [12] D. B. Keator, K. Helmer, J. Steffener, J. A. Turner, T. G. Van Erp, S. Gadde, *et al.*, "Towards structured sharing of raw and derived neuroimaging data across existing resources," *Neuroimage*, vol. 82, pp. 647-61, Nov 15 2013.

- [13] R. L. Harrigan, B. C. Yvernault, B. D. Boyd, S. M. Damon, K. D. Gibney, B. N. Conrad, *et al.*, "Vanderbilt University Institute of Imaging Science Center for Computational Imaging XNAT: A multimodal data archive and processing environment," *Neuroimage*, vol. 124, pp. 1097-101, Jan 01 2016.
- [14] A. Scott, W. Courtney, D. Wood, R. de la Garza, S. Lane, M. King, *et al.*, "COINS: An Innovative Informatics and Neuroimaging Tool Suite Built for Large Heterogeneous Datasets," *Front Neuroinform*, vol. 5, p. 33, 2011.
- [15] A. Assoc, "2012 Alzheimer's disease facts and figures," *Alzheimers & Dementia*, vol. 8, pp. 131-168, Mar 2012.
- [16] B. Dubois, H. H. Feldman, C. Jacova, H. Hampel, J. L. Molinuevo, K. Blennow, *et al.*, "Advancing research diagnostic criteria for Alzheimer's disease: the IWG-2 criteria," *Lancet Neurology*, vol. 13, pp. 614-629, Jun 2014.
- [17] B. Fischl, "FreeSurfer," *Neuroimage*, vol. 62, pp. 774-81, Aug 15 2012.
- [18] M. Larobina and L. Murino, "Medical image file formats," *J Digit Imaging*, vol. 27, pp. 200-6, Apr 2014.
- [19] S. M. Smith, M. Jenkinson, M. W. Woolrich, C. F. Beckmann, T. E. Behrens, H. Johansen-Berg, *et al.*, "Advances in functional and structural MR image analysis and implementation as FSL," *Neuroimage*, vol. 23 Suppl 1, pp. S208-19, 2004.
- [20] C. C. Chang and C. J. Lin, "LIBSVM: A Library for Support Vector Machines," *Acm Transactions on Intelligent Systems and Technology*, vol. 2, 2011.
- [21] G. G. Fillenbaum, "Concomitants of Mini-Mental Status Examination (Mmse) Score," *Gerontologist*, vol. 26, pp. A83-A83, Oct 1986.
- [22] C. C. Rowe, U. Ackerman, W. Browne, R. Mulligan, K. L. Pike, G. O'Keefe, *et al.*, "Imaging of amyloid beta in Alzheimer's disease with F-18-BAY94-9172, a novel PET tracer: proof of mechanism," *Lancet Neurology*, vol. 7, pp. 129-135, Feb 2008.
- [23] C. C. Rowe, V. Dore, G. Jones, D. Baxendale, R. S. Mulligan, S. Bullich, *et al.*, "F-18-Florbetaben PET beta-amyloid binding expressed in Centiloids," *European Journal of Nuclear Medicine and Molecular Imaging*, vol. 44, pp. 2053-2059, Nov 2017.
- [24] W. E. Klunk, R. A. Koeppe, J. C. Price, T. L. Benzinger, M. D. Devous, W. J. Jagust, *et al.*, "The Centiloid Project: Standardizing quantitative amyloid plaque estimation by PET," *Alzheimers & Dementia*, vol. 11, pp. 1-15, Jan 2015.
- [25] E. H. Gronenschild, P. Habets, H. I. Jacobs, R. Mengelers, N. Rozendaal, J. van Os, *et al.*, "The effects of FreeSurfer version, workstation type, and Macintosh operating system version on anatomical volume and cortical thickness measurements," *PLoS One*, vol. 7, p. e38234, 2012.
- [26] A. Pfefferbaum, T. Rohlfing, M. J. Rosenbloom, and E. V. Sullivan, "Combining atlas-based parcellation of regional brain data acquired across scanners at 1.5 T and 3.0 T field strengths," *Neuroimage*, vol. 60, pp. 940-51, Apr 02 2012.

- [27] S. Bullich, V. L. Villemagne, A. M. Catafau, A. Jovalekic, N. Koglin, C. C. Rowe, *et al.*, "Optimal Reference Region to Measure Longitudinal Amyloid-beta Change with F-18-Florbetaben PET," *Journal of Nuclear Medicine*, vol. 58, pp. 1300-1306, Aug 1 2017.
- [28] E. Morris, A. Chalkidou, A. Hammers, J. Peacock, J. Summers, and S. Keevil, "Diagnostic accuracy of (18)F amyloid PET tracers for the diagnosis of Alzheimer's disease: a systematic review and meta-analysis," *Eur J Nucl Med Mol Imaging*, vol. 43, pp. 374-85, Feb 2016.
- [29] I. Sarikaya, "PET studies in epilepsy," *Am J Nucl Med Mol Imaging*, vol. 5, pp. 416-30, 2015.
- [30] M. M. Miller-Thomas and T. L. Benzinger, "Neurologic Applications of PET/MR Imaging," *Magn Reson Imaging Clin N Am*, vol. 25, pp. 297-313, May 2017.
- [31] K. Krupa and M. Bekiesinska-Figatowska, "Artifacts in Magnetic Resonance Imaging," *Polish Journal of Radiology*, vol. 80, pp. 93-106, 2015.
- [32] U. Vovk, F. Pernus, and B. Likar, "A review of methods for correction of intensity inhomogeneity in MRI," *Ieee Transactions on Medical Imaging*, vol. 26, pp. 405-421, Mar 2007.
- [33] G. Delso, A. Martinez-Moller, R. A. Bundschuh, S. G. Nekolla, and S. I. Ziegler, "The effect of limited MR field of view in MR/PET attenuation correction," *Medical Physics*, vol. 37, pp. 2804-2812, Jun 2010.
- [34] C. R. Jack, M. A. Bernstein, N. C. Fox, P. Thompson, G. Alexander, D. Harvey, *et al.*, "The Alzheimer's Disease Neuroimaging Initiative (ADNI): MRI methods," *Journal of Magnetic Resonance Imaging*, vol. 27, pp. 685-691, Apr 2008.
- [35] R. Nordenskjold, F. Malmberg, E. M. Larsson, A. Simmons, S. J. Brooks, L. Lind, *et al.*, "Intracranial volume estimated with commonly used methods could introduce bias in studies including brain volume measurements," *Neuroimage*, vol. 83, pp. 355-360, Dec 2013.
- [36] J. D. Gispert, S. Reig, J. Pascau, J. J. Vaquero, P. Garcia-Barreno, and M. Desco, "Method for bias field correction of brain T1-weighted magnetic resonance images minimizing segmentation error," *Human Brain Mapping*, vol. 22, pp. 133-144, Jun 2004.
- [37] S. S. Chandra, C. Engstrom, J. Fripp, A. Neubert, J. Jin, D. Walker, *et al.*, "Local contrast-enhanced MR images via high dynamic range processing," *Magnetic Resonance in Medicine*, vol. 80, pp. 1206-1218, Sep 2018.
- [38] D. Q. Zhang, Y. P. Wang, L. P. Zhou, H. Yuan, D. G. Shen, and A. D. N. Initia, "Multimodal classification of Alzheimer's disease and mild cognitive impairment," *Neuroimage*, vol. 55, pp. 856-867, Apr 1 2011.
- [39] B. Magnin, L. Mesrob, S. Kinkingnehun, M. Pelegrini-Issac, O. Colliot, M. Sarazin, *et al.*, "Support vector machine-based classification of Alzheimer's

- disease from whole-brain anatomical MRI," *Neuroradiology*, vol. 51, pp. 73-83, Feb 2009.
- [40] S. Kloppel, C. M. Stonnington, C. Chu, B. Draganski, R. I. Scahill, J. D. Rohrer, *et al.*, "Automatic classification of MR scans in Alzheimers disease," *Brain*, vol. 131, pp. 681-689, Mar 2008.
- [41] K. B. Walhovd, A. M. Fjell, J. Brewer, L. K. McEvoy, C. Fennema-Notestine, D. J. Hagler, *et al.*, "Combining MR Imaging, Positron-Emission Tomography, and CSF Biomarkers in the Diagnosis and Prognosis of Alzheimer Disease," *American Journal of Neuroradiology*, vol. 31, pp. 347-354, Feb 2010.
- [42] R. Cuingnet, E. Gerardin, J. Tessieras, G. Auzias, S. Lehericy, M. O. Habert, *et al.*, "Automatic classification of patients with Alzheimer's disease from structural MRI: A comparison of ten methods using the ADNI database," *Neuroimage*, vol. 56, pp. 766-781, May 15 2011.
- [43] Q. Zhou, M. Goryawala, M. Cabrerizo, J. Wang, W. Barker, D. A. Loewenstein, *et al.*, "An Optimal Decisional Space for the Classification of Alzheimer's Disease and Mild Cognitive Impairment," *Ieee Transactions on Biomedical Engineering*, vol. 61, pp. 2245-2253, Aug 2014.
- [44] J. L. Chepkoech, K. B. Walhovd, H. Grydeland, A. M. Fjell, and I. Alzheimer's Disease Neuroimaging, "Effects of change in FreeSurfer version on classification accuracy of patients with Alzheimer's disease and mild cognitive impairment," *Hum Brain Mapp*, vol. 37, pp. 1831-41, May 2016.
- [45] W. J. Jagust, S. M. Landau, R. A. Koeppe, E. M. Reiman, K. Chen, C. A. Mathis, *et al.*, "The Alzheimer's Disease Neuroimaging Initiative 2 PET Core: 2015," *Alzheimers Dement*, vol. 11, pp. 757-71, Jul 2015.

## VITA

### GABRIEL LIZARRAGA

#### EDUCATION

- 1976      Born, Havana, Cuba
- 2010      B.S., Computer Science  
Florida International University  
Miami, FL
- 2011      M.S., Computer Science  
Florida International University  
Miami, FL
- 2015      Ph.D. Candidate, Computer Science  
Florida International University  
Miami, Florida

#### PUBLICATIONS

G. Lizarraga, C. Li, M. Cabrerizo, W. Barker, D.A. Loewenstein, R. Duara, and Malek Adjouadi, A Neuroimaging Web Services Interface as a Cyber Physical System for Medical Imaging and Data Management in Brain Research: Design Study, *JMIR Med Inform.* Vol. 6 (2), pp: 228-244, February 2018.

R.E. Curiel, D.A. Loewenstein, M. Rosselli, A. Penate, M.T. Greig-Custo, R.M. Bauer, S. M. Guinjoan, K.S. Hanson, C. Li, G. Lizarraga, W. Barker, V. Torres, S. DeKosky, M. Adjouadi, and R. Duara, "Semantic Intrusions and Failure to Recover from Semantic Interference in Mild Cognitive Impairment: Relationship to Amyloid and Cortical Thickness", *Current Alzheimer Research*, Vol. 15 (9), pp. 848-855, 2018.

D. A. Loewenstein, R. E. Curiel, S.DeKosky, R. M. Bauer, M. Rosselli, S. M. Guinjoan, M. Adjouadi, A. Peñate, W. W. Barker, S. Goenaga, T. Golde, M. T. Greig-Custo, K. S. Hanson, C. Li, G. Lizarraga, M. Marsiske, R. Duara, Utilizing Semantic Intrusions to Identify Amyloid Positivity in Mild Cognitive Impairment, *Neurology*, *Neurology*. 91. 10.1212/WNL.0000000000006128. 10.1212/WNL.0000000000006128, August 2018.

D. A. Loewenstein, R. E. Curiel, S. DeKosky, M. Roselli, R. Bauer, M. Grieg-Custo, A. Penate, C. Li, G. Lizarraga, T. Golde, M. Adjouadi, and R. Duara, Recovery from proactive semantic interference and MRI volume: A replication and extension study, *Journal of Alzheimer's Disease*. Vol 59 issue 1, pp 131-139, 2017

L. Lattari, A. Montenegro, A. Conci, E.W. Clua, V.F. Mota, M. B. Vieira, and G. Lizarraga, Using Graph Cuts in GPUs for Color Based Human Skin Segmentation, Integrated Computer-Aided Engineering Journal. Vol 18 issue 1, 2011.

A. Pinzon, M. Cabrerizo, G. Lizarraga, B. Wolf, C. Vallin, S. Garcia, and M. Adjouadi, "EEG (Ictal and Inter-Ictal) Connectivity Patterns and 3-D Spike Source Analysis In Focal Epilepsy and its Relation to Nuclear Medicine Imaging", 32nd International Epilepsy Congress, Barcelona, Spain, September 02-06, 2017, appearing in Epilepsia, Vol. 58, Supplement 5, pp. S34-S35, Dec. 2017.

M. Adjouadi, M. Ayala, M. Cabrerizo, A. Zong, G. Lizarraga, and M. Rossman, "Classification of Leukemia Blood Samples Using Neural Networks", Annals of Biomedical Engineering, Vol. 38 (4), pp. 1473-1482, April 2010.

G. Lizarraga, M. Cabrerizo, R. Duara, N. Rojas, M. Adjouadi and D. Loewenstein, A Web Platform for data acquisition and analysis for Alzheimer's disease, SoutheastCon 2016, Norfolk, VA, 2016, pp. 1-5. doi: 10.1109/SECON.2016.7506730

A Gordon, M. Hines, D Da Silva, M Ben-Yehuda, G Lizarraga, Automated, Application-Driven Memory Over commitment for Cloud Computing Runtime Environments/Systems, Layering, and Virtualized Environments Workshop, 2011

G. Lizarraga, M. Cabrerizo, M. Ayala, M. Adjouadi, "Parallelized and Multithreaded FFT Applied to Extraction of EEG Data Key Parameters Towards Seizure Detection and Prediction", Proceedings of the SACNAS National Conference, pp. 179, Oct 15-18, 2009, Dallas, TX

M. Guillen, M. Adjouadi, B. Bernal, M. Ayala, A. Barreto, N. Rishe, G. Lizarraga, X. You, W. Gaillard, "A Knowledge-Based Database System for Visual Rating of fMRI Activation Patterns for Brain Language Networks", The Fifth Richard Tapia Celebration of Diversity in Computing Conference: Intellect, Initiatives, Insight, and Innovations, pp. 1-6, 2009, Portland, OR

G. Lizarraga, M. Adjouadi, M. Cabrerizo, M. Ayala, M. Tito, "Integration of Dipole Model and Current Density Reconstruction towards 3-D Source Localization using EEG and MRI", Proceedings of the CAHSI Annual Meeting, pp. 4-7, Jan 15-18, 2009, Google headquarters, Mountain View, CA

M. Tito, M. Adjouadi, M. Cabrerizo, M. Ayala, and G. Lizarraga, "Detecting Seizures Using Gamma-Range Power Measurements and Nonlinear Decision Functions", Proceedings of the CAHSI Annual Meeting, pp. 13-17, Jan 15-18, 2009, Google headquarters, Mountain View, CA